

2011

Structure And Surface Alloying of Sn on a Pt(110) Single Crystal

Jie Fu

Lehigh University

Follow this and additional works at: <http://preserve.lehigh.edu/etd>

Recommended Citation

Fu, Jie, "Structure And Surface Alloying of Sn on a Pt(110) Single Crystal" (2011). *Theses and Dissertations*. Paper 1330.

This Thesis is brought to you for free and open access by Lehigh Preserve. It has been accepted for inclusion in Theses and Dissertations by an authorized administrator of Lehigh Preserve. For more information, please contact preserve@lehigh.edu.

Structure And Surface Alloying of Sn on a Pt(110) Single Crystal

by

Jie Fu

A Thesis

Presented to the Graduate and Research Committee

of Lehigh University

in Candidacy for the Degree of

Master of Sciences

in

Chemistry Department

Lehigh University

August 7, 2011

© 2011 Copyright

Jie Fu

Thesis is accepted and approved in partial fulfillment of the requirements for the Master of Science in Chemistry Department.

Structure and surface alloying of Sn on a Pt(110) single crystal

Jie Fu

Date Approved

Bruce E. Koel

Thesis Advisor

Robert A. Flowers, II

Department Chairman

ACKNOWLEDGMENTS

I wish to express my special thanks to Prof. Bruce E. Koel for taking me as his student and giving valuable advices during my research. I would like to thank Dr. Xiaofang Yang for teaching me plentiful lab skills and experience, and my lab mates Dr. Lindsey Welch and Dr. Mauricio Ramos for your generous help and accompanying..

I would also like to thank my committee members, Prof. Jim Roberts, Prof. David Moore, Prof. Israel Wachs, and Dr. Rebecca Miller and all the nice people and friends in Lehigh Chemistry Department.

At last I want to thank my husband, Dong Li. Without you, I would not be able to accomplish my thesis and get the degree.

TABLE OF CONTENTS

LIST OF FIGURES	vii
LIST OF TABLES	ix
ABSTRACT	1
Chapter 1 Introduction.....	2
1.1 Background.....	2
1.2 Overview.....	2
Chapter 2 Experimental Methods.....	5
2.1 UHV Scanning Tunneling Microscope System.....	5
2.2 Sample Preparation.....	7
2.3 Surface Analytical Techniques	10
2.3.1 LEED.....	10
2.3.2 XPS and AES	10
2.3.3 LEIS	12
2.3.4 STM.....	13
Chapter 3 Structure of the Clean Pt (110) Single Crystal Surface	17
3.1 Introduction.....	17
3.2 Experimental Methods.....	18
3.3 Results and Discussion	19
3.4 Conclusions.....	21
Chapter 4 Structure of Sn/Pt(110) Surfaces with Medium Sn Coverage	22
4.1 Introduction.....	22
4.2 Experimental Methods.....	23
4.3 Results and Discussion	23
4.3.1 Determination of the Sn coverage.....	23
4.3.2 Temperature Influence on Surface Composition	26

4.3.3 STM Results.....	27
4.4 Conclusions.....	29
Chapter 5 Structure of Sn/Pt(110) Surfaces with High Sn Coverage.....	31
5.1 Introduction.....	31
5.2 Experimental Details.....	31
5.3 Results and Discussion	32
5.3.1 Temperature Influence on Surface Composition	32
5.3.2 LEED Results.....	33
5.3.3 STM Results.....	34
5.4 Conclusions.....	46
Chapter 6 Conclusions.....	47
References	48
Vita	52

LIST OF FIGURES

Figure 1.1 Structure of the (2×2) Sn-Pt(111), $(\sqrt{3} \times \sqrt{3})R30^\circ$ Sn-Pt(111) and $c(2 \times 2)$ Sn-Pt(100) surface alloys.	3
Figure 2.1 Picture of the RHK STM system.	5
Figure 2.2 Schematic drawings of the RHK STM system.	6
Figure 2.3 A picture of RHK STM scanning chamber and schematic drawing of the STM scanner head. ²⁴	6
Figure 2.4 Schematic drawing showing the RHK sample holder.	8
Figure 2.5 Sn uptake curves obtained from a Pt(111) single crystal.....	9
Figure 2.6 Schematic drawing of x-ray excitation of photoelectrons and Auger electrons. ³⁰	11
Figure 2.7 Schematic drawing of the incident ion interaction in LEIS.....	13
Figure 2.8 Scanning modes for STM, adapted from ref 30.....	15
Figure 3.1 Structure of the clean Pt(110)- (1×2) missing row reconstruction.....	18
Figure 3.2 A and B: Clean Pt(110) surface with the (1×2) missing-row reconstruction.	20
Figure 4.1 STM image of Pt(110)-Sn surface at 0.4 ML Sn coverage.....	22
Figure 4.2 LEIS spectra of Sn-deposited Pt(110) surface with increased Sn exposure ²⁴	24
Figure 4.3 XPS uptake curves for Sn deposited on a Pt(110) surface.....	25
Figure 4.4 Surface Sn concentration varies with annealing temperature.	26

Figure 4.5 STM images of 1-ML Sn/Pt(110) surface annealed to 750 K for 3 min	29
Figure 4.6 STM images of 1-ML Sn/Pt(110) annealed to 1000 K for 3min	29
Figure 5.1 Surface Sn concentration varies with annealing temperature.	32
Figure 5.2 LEED pattern evolution of Sn alloying process.....	33
Figure 5.3 STM images of 2.7-ML Sn/Pt (110), as-deposited.	34
Figure 5.4 STM images of 2.7-ML Sn/Pt (110) after annealed to 600 K.....	36
Figure 5.5 STM images of 2.7-ML Sn/Pt (110) after annealed to 600 K.....	37
Figure 5.6 Cross-sectional view of line a and b in Figure 5.5.....	37
Figure 5.7 STM images of 2.7-ML Sn/Pt (110) after annealed to 700 K.....	39
Figure 5.8 STM images of 2.7-ML Sn/Pt (110) after annealed to 900 K.....	40
Figure 5.9 STM images of 2.7-ML Sn/Pt (110) after annealed to 900 K.....	40
Figure 5.10 Possible model of 2.7-ML Sn/Pt(110) surface at 900 K.....	41
Figure 5.11 STM images of 2.7-ML Sn/Pt (110) after annealed to 1000 K.....	42
Figure 5.12 STM images of 2.7-ML Sn/Pt (110) after annealed to 1050 K.....	43
Figure 5.13 STM image of Pt ₃ Sn(110) single crystal after annealing to 1000 K.....	44

LIST OF TABLES

Table 3.1 Comparison of distances obtained directly from STM images and from a lattice model	21
Table 5.1 Proposed models for each alloy surfaces	45

ABSTRACT

The structure and chemistry of Pt-Sn alloy surfaces is of interest for a number of catalytic and electrocatalytic applications. Previous research showed that low coverage of Sn tends to form 1D Pt-Sn-Pt alloy chains on the Pt(110) surface at room temperature, but no significant change was observed from low energy electron diffraction (LEED). These chains dissolve into the bulk after annealing to 900 K and leave a disordered surface. Our studies using scanning tunneling microscopy (STM), LEED, low energy ion scattering (LEIS) and X-ray photoelectron spectroscopy (XPS) show that Sn will alloy with Pt(110) at room temperature and when the exposure is getting larger, the surface will change its preferred growing direction. High temperature annealing (greater than 1000 K) will make a Sn-rich surface alloy analogue to a Pt₃Sn(110) bulk alloy single crystal surface.

Chapter 1 Introduction

1.1 Background

Heterogeneous catalysts have been used extensively in chemical and petroleum industry and the bimetallic alloy is one of the main streams. By varying the components and their compositions, people can tune the active sites of the catalysts and improve both their reactivity and stability comparing to the single component ones. The ultrahigh vacuum (UHV) environment required by most surface science techniques is a great mimic and can reduce the complexity of the real catalytic reactions, although it seems less like the real circumstance where catalytic reactions happen. The surface science study will provide the fundamental understanding of each reaction occurring on the catalysts surface and be the guide for choosing suitable catalysts. Therefore, studying the bimetallic alloy catalysts has always been a goal for surface scientists.

The surface structure of a certain catalyst plays important roles in governing its reactivity. The number and the nature of edges, kinks, steps, defects and the way two elements alloying with each other will ultimately change the reaction pathways. Revealing the surface structure is the first step towards understanding the catalytic reactions. That is the objective of this thesis, to study the surface structure of Sn-Pt(110) bimetallic surface alloy.

1.2 Overview

Pt-Sn bimetallic surface alloys have been well studied for decades. On the most stable low index phase, Pt(111) surface, two distinct surface alloys are formed^{1,2}. The

(2×2) alloy has ensembles of five Pt atoms and 3-fold pure Pt hollow sites, and the $(\sqrt{3} \times \sqrt{3})R30^\circ$ alloy has only ensembles of four Pt atoms and 2-fold pure Pt bridging sites. On Pt(100) surface, a $c(2 \times 2)$ overlayer of Sn-Pt alloy is often observed, while the $(3\sqrt{2} \times \sqrt{2})R45^\circ$ alloy can also be formed when annealing samples at higher temperatures^{3,4}. The schematic illustrations of these structures are shown in Figure 1.1.

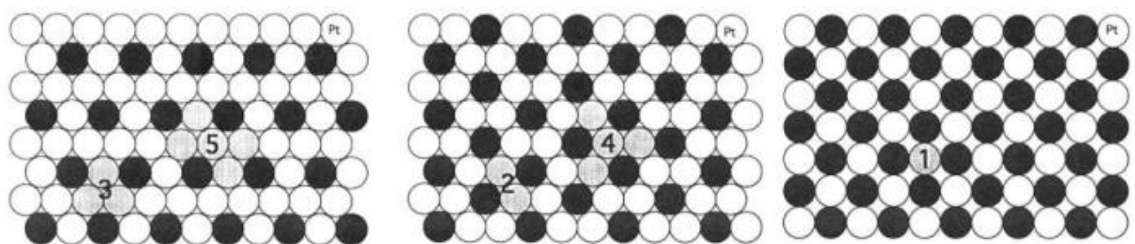


Figure 1.1 Structure of the (2×2) Sn-Pt(111), $(\sqrt{3} \times \sqrt{3})R30^\circ$ Sn-Pt(111) and $c(2 \times 2)$ Sn-Pt(100) surface alloys.

Reactions on these surface alloys, such as hydrogenation of α, β -unsaturated aldehydes, hydrogenation of dienes and alkynes, dehydrogenation of paraffins and oxidation of alkanes have been mostly studied by our group and some other research groups.^{5-13 14} In general, Sn-Pt alloys show lower activity and higher selectivity towards some unsaturated molecules and oxygen-containing reactions compared to Pt single crystals. This is due to a decreased concentration of Pt on the surface which has higher binding energy with carbon and an increased amount of Sn which bonds with oxygen stronger.

However another low index face of Pt(110) has only drawn little attention. It has been reported that Mn¹⁵, Co¹⁶⁻¹⁸, Ni^{19,20}, Rh²¹, Ag²², etc were used to grow on Pt(110) single crystal surface. X-ray photoelectron diffraction (XPD) shows that the multi-

atomic layer cobalt film is ordered and has a well-defined epitaxial relationship with the Pt(110) substrate.¹⁷ Most of these studies also agree that the initial growth of the second metal element on the Pt(110) surface follows the Stranski-Krastanov (S-K) mode in which second metal element first fill up the missing rows and grow to 1.5 monolayer epitaxial film followed by an agglomeration into three dimensional islands.

For Sn-Pt(110) system, there is only one report published discussing about the corrosive adsorption of small amount of Sn onto the Pt(110) surface.²³ It is shown that adding 0.4 ML Sn to a clean Pt(110) surface caused formation of three different configurations at room temperature: alloyed Pt–Sn–Pt chains, mobile Sn ad-atoms in the valley of the missing row reconstruction, and small 3D Pt–Sn alloy islands. The islands formed before the valleys were completely filled and the alloyed Pt-Sn-Pt chains were not detected by LEED.

In order to get a complete view of the interaction between Sn and Pt(110) surface, we designed and performed a series of experiments with two additional coverages of Sn on Pt(110), near monolayer (ML) and two monolayers (MLs), which are denoted as medium coverage and high coverage respectively in this thesis. Surface analytical methods including low energy electron diffraction (LEED), x-ray photoelectron spectroscopy (XPS), auger electron spectroscopy (AES), low energy ion scattering spectroscopy (LEIS) and scanning tunneling microscopy (STM) were utilized to investigate the surface composition and probe the surface structure. This work provided us with a comprehensive understanding of Sn-Pt(110) bimetallic surface alloy system and allowed us to further explore the chemistry and reactivity of this surface alloy.

Chapter 2 Experimental Methods

2.1 UHV Scanning Tunneling Microscope System

All of the experiments described in this thesis were conducted by using a commercial RHK UHV 3000 STM system with a base pressure of 2×10^{-10} torr following bakeout. The system is equipped with surface analytical techniques, such as LEED, XPS, AES, LEIS, quadrupole mass spectrometer (QMS), ion sputtering gun for sample cleaning, leak valves, and resistively heated Sn doser made using a Ta-boat, and STM probe with variable temperature control sample stage. The picture and schematic drawing of the system are shown in Figure 2.1 and Figure 2.2.

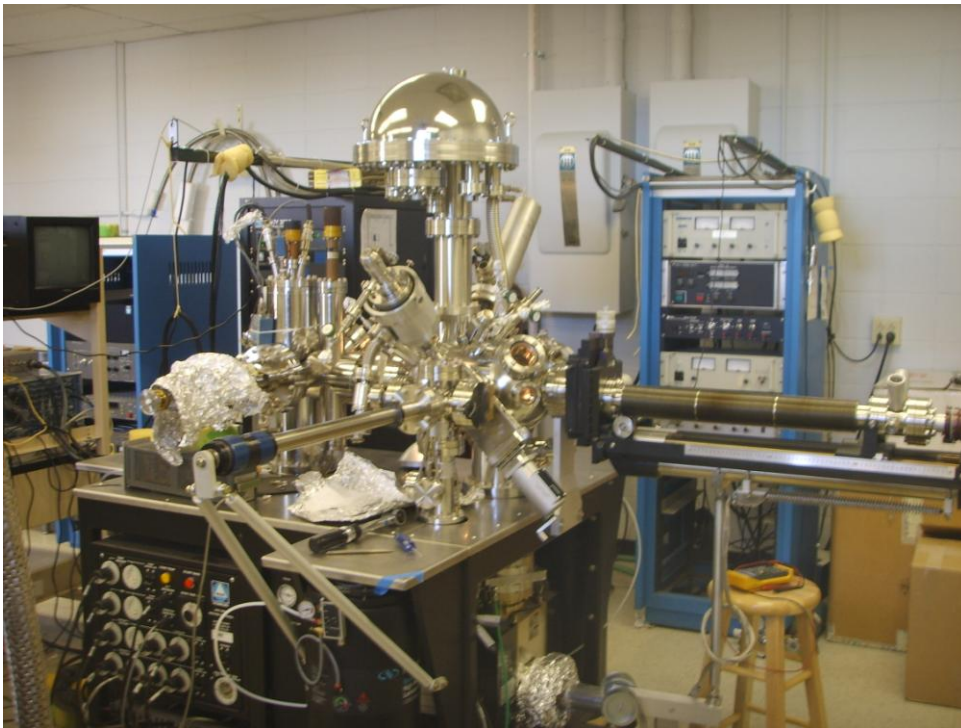


Figure 2.1 Picture of the RHK STM system.

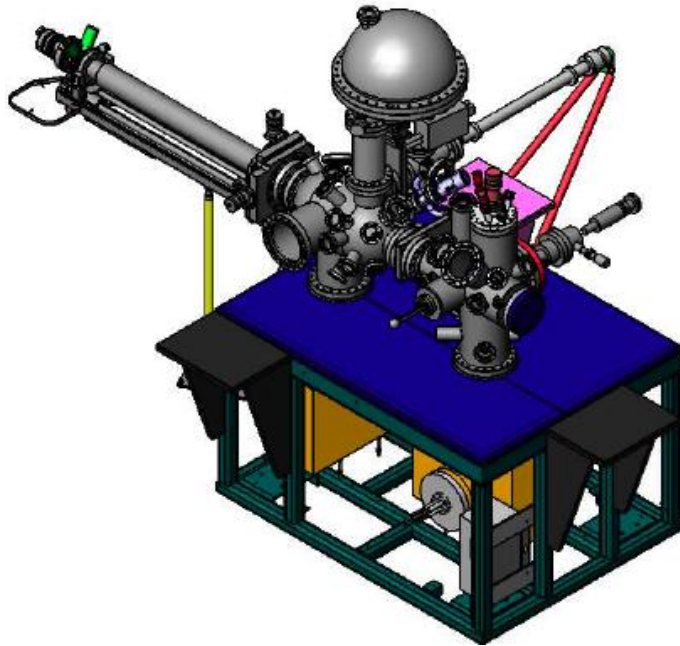


Figure 2.2 Schematic drawings of the RHK STM system.

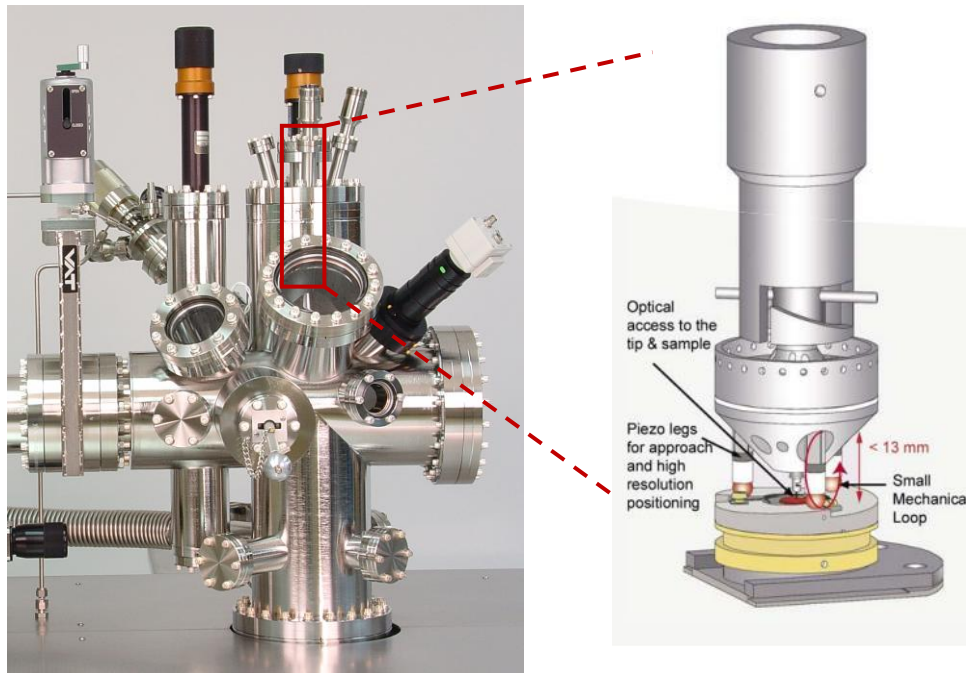


Figure 2.3 A picture of RHK STM scanning chamber and schematic drawing of the STM scanner head.²⁴

The STM scanner head is based on the so-called “Johnny Walker” Beetle™ design, which is the most mechanically and thermally stable of the many STM designs. Figure 2.3 shows the geometry of the scanner head design and its interaction with the sample holder ramp.

2.2 Sample Preparation

Standard procedures for cleaning the Pt single crystal and preparing the Sn/Pt(110) surface alloys were used.^{1,4} The Pt(110) single crystal was cleaned by using cycles of 500 - 1000 eV Ar⁺ ion (5×10^{-5} Torr) sputtering to remove the residual Sn. XPS and AES were used to check the Sn contamination level. When the Sn 3d over Pt 4f XPS peak area ratio is no longer decreasing (ratio value is around 0.02 or less) the sputtering process was complete. Carbon residues left on the surface were removed by annealing the sample at 600 ~ 800 K in $\sim 5 \times 10^{-8}$ Torr O₂ for few minutes. The sample was transferred directly under the nozzle of O₂ doser at this step. The sample was then flashed to 1200 K for 10 seconds to form the Pt(110)-(1×2) reconstructed surface.^{25,26} The cleanliness of the sample was checked using LEIS and XPS and the surface ordering was confirmed using LEED.

Sample was heated by radiation heating for $T < 700$ K and e-beam heating for a higher range. A typical sample holder used in the experiment is shown in Figure 2.4, in which the Quartz lamp was replaced by a 60 W filament and the e-beam heating was accomplished by applying bias between the filament and the sample. The sample was

allowed to cool down to room temperature before each time we performed the Sn dosing and the STM imaging.

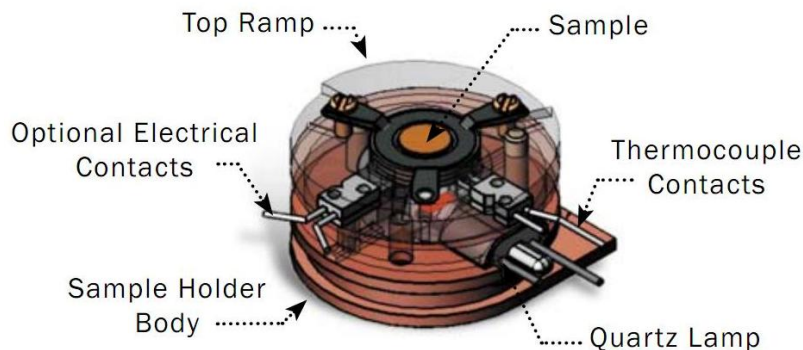


Figure 2.4 Schematic drawing showing the RHK sample holder. Taken from ref 27²⁷.

Deposition of Sn was accomplished through a homemade Sn doser. The Sn doser was built by using a 2-conductor, high-voltage, electrical feed-through mounted on a 2.75-in Conflat™ flange. A resistively heated Ta “boat” containing high purity Sn (6N) was suspended between two 0.010-in Ta wires that were spot-welded to the Cu feed-throughs. The diameter of the pinhole in the Ta sheet covering the Ta-boat was 0.5 mm. A stainless steel foil shield and tube were attached to one of the Cu rods and positioned directly above the pinhole to restrict the path of Sn to the sample region. The boat was heated resistively using a DC power supply. Sn coverage was monitored and determined by comparison to a Sn/Pt XPS uptake plot performed for a Pt(111) single crystal under otherwise identical conditions. As shown in Figure 2.5, a “break” in this curve for completion of the Sn monolayer occurred at Dosing time = 2 min which gave a Sn(3d)/Pt(4f) XPS peak ratio of 0.18. The Sn(3d) in this work stands for the area under

both Sn 3d 5/2 and Sn 3d 3/2 peaks, and the Pt(4f) represents the sum of peak areas of both Pt 4f 7/2 and Pt 4f 5/2. The atomic sensitivity factor was not corrected since we were only interested at the ratio. Therefore 1 ML of Sn on Pt(111) was assigned when the Sn(3d)/Pt(4f) XPS peak ratio equals 0.18. An AES uptake curve was also performed (not shown) and consistent with XPS results.

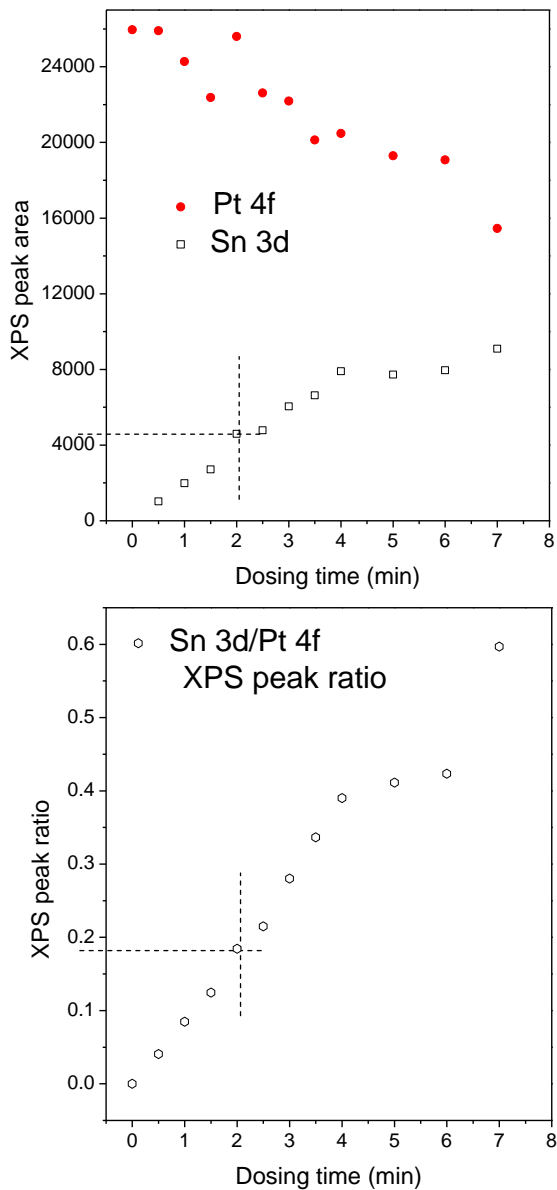


Figure 2.5 Sn uptake curves obtained from a Pt(111) single crystal.

2.3 Surface Analytical Techniques

2.3.1 LEED

LEED is one of most common surface techniques for determining the surface structure of crystalline materials.²⁸ Incident low energy electrons (20-200eV) beam bombards with the surface atoms and the diffracted electrons will display certain pattern on a fluorescent screen depending on the crystalline and uniformity. LEED can be used both qualitatively and quantitatively, which means to analyze the diffraction pattern and the intensities of diffraction beams respectively. In this work, LEED was mainly adopted as a convenient visual tool to examine the surface orderliness and to reveal the crystalline change when the alloying occurs.

2.3.2 XPS and AES

X-ray photoelectrons and Auger electrons can be explained and compared in one process.²⁹ When a photon with energy $h\nu$ enters the surface and hits a core-level electron with a binding energy E_b , the electron will be ejected with a kinetic energy $KE = h\nu - E_b$ and is the photoelectron (*eg.* The photoejected K-shell electron in Figure 2.6 left³⁰). One outer level electron falls off to the empty site on the core level and releases energy which is then absorbed by another valence level electron. The latter one gaining extra energy and jumping out to vacuum level is the so called Auger electron (*eg.* The Auger electron ejected from L_{23} shell in Figure 2.6 right³⁰). It is obvious that both photoelectrons and Auger electrons are directly related to the atomic nature, such as binding energy and the

energy gap between each level. By monitoring the kinetic energy of out-coming electrons, one can determine the composition and chemical state of the target surface.

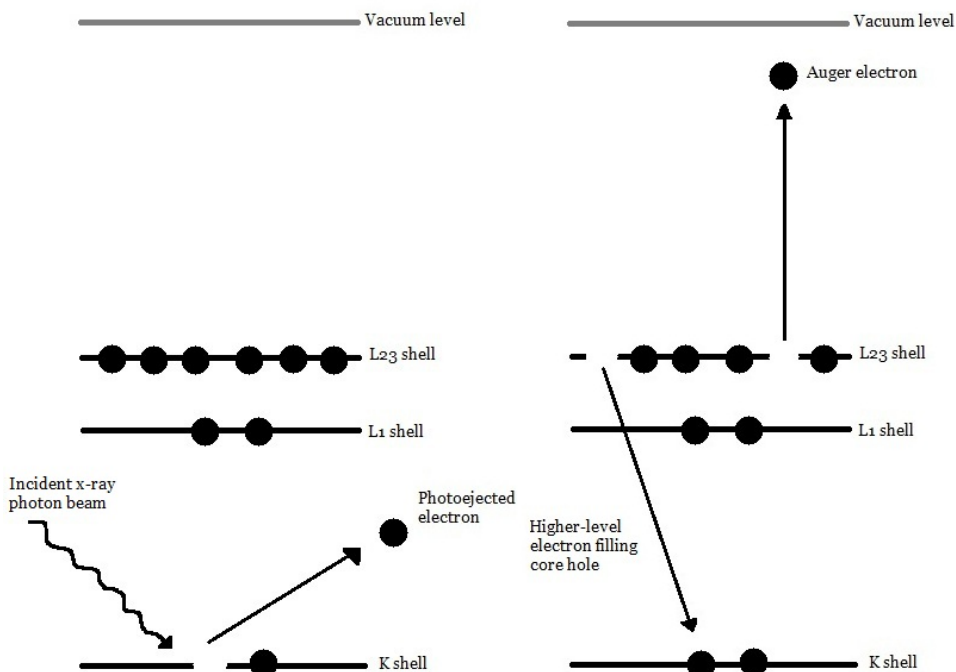


Figure 2.6 Schematic drawing of x-ray excitation of photoelectrons and Auger electrons.³⁰

In practice, X-ray source photon energy is usually restricted to two lines, the Al and Mg K_{α} X-ray emissions at 1486.6 eV and 1253.6 eV, respectively. The kinetic energies of generated photoelectrons are within 0 - 1486.6 eV which corresponding to an electron mean free path of ~ 1 nm. Auger electrons are produced more easily by shooting an energetic electron beam (1.5 - 5 keV) and the detected energies are usually 0 - 800 eV. This lower kinetic energy feature means AES is more surface-sensitive and often used for determining the surface contamination level and the thickness and composition changes when studying the bimetallic systems.

In studies of thin film growth, AES and XPS intensities are used along with equations such as that in Eqn. (1)³¹ that accounts for the electron mean free path and surface sensitivity

$$\frac{(I_A/s_A)}{(I_B/s_B)} = \frac{1 - \exp [-d/\lambda_{imfp}^A(E_A) \cos \theta]}{\exp [-d/\lambda_{imfp}^A(E_B) \cos \theta]} \quad \text{Eqn. (1)}$$

where I is the intensity of electrons that is expected to observe from an overlayer of thickness d , s_A is sensitive factor, λ_{imfp} is the inelastic mean free path (IMFP) of electrons which is a function of kinetic energy E_A of the Auger or photoelectrons from the overlayer, θ is the emission angel.

In this work, a Mg K_α X-ray (1253.6 eV) beam was utilized as the x-ray source and a single channel hemisphere analyzer was used to detect the photoelectrons. As shown in Section 2.2, by preparing the uptake curve of Sn on Pt(111), we can determine the coverage of deposited Sn films. The same procedure was carried out on Pt(110) crystal and the results will be summarized in Chapter 4.

2.3.3 LEIS

When a light incident ion (mass = m_1) strikes the heavy surface atom (mass = m_2), it will bounce off the surface and obey the energy conservation law where the outgoing energy E_f is governed by the incident energy E_0 , scattering angle θ , and atomic weight ratio m_2/m_1 (Figure 2.7).³² This is the basis of LEIS.

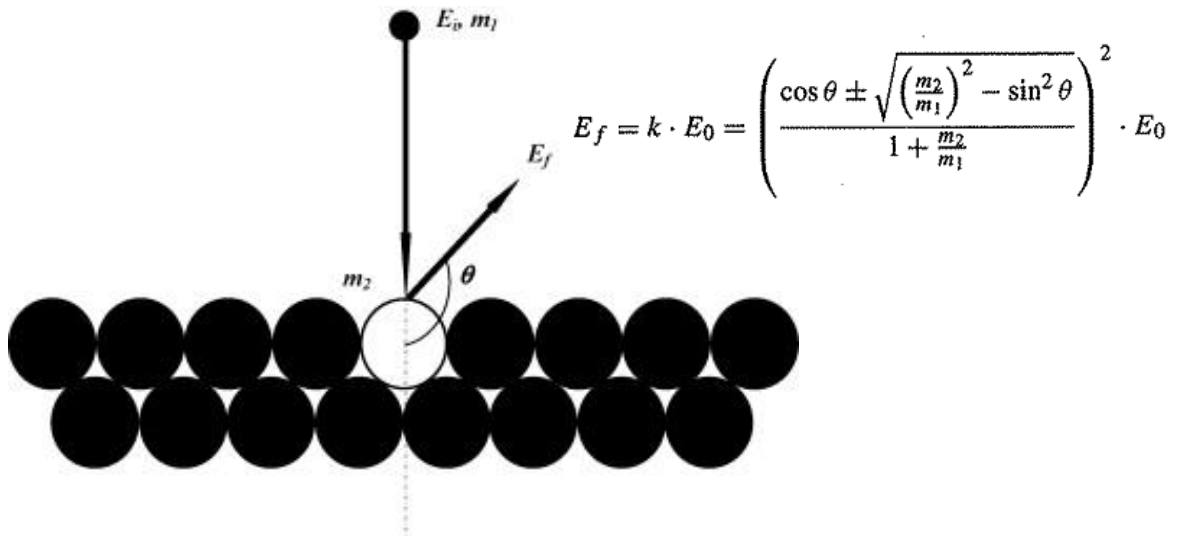


Figure 2.7 Schematic drawing of the incident ion interaction in LEIS.

Since only the ions collided with the first atomic layer of the surface can be detected, LEIS is more surface sensitive than both AES and XPS. If element B grows on substrate A in a layer-by-layer model, we can determine the coverage of B by watching the signal decreasing of A and increasing of B in the uptake curve. When 1 ML of B completely covers the surface, the peak from element A will no longer be observed. However, our research showed that Sn will alloy with Pt(110) surface at room temperature and the growth pattern is not layer-by-layer. Thus the LEIS cannot be the conclusive evidence of determination of the Sn coverage in this work.

For a typical LEIS experiment, we used 1 keV He^+ ($p = 5 \times 10^{-8}$ torr) ion with as incident beam and scattering angle $\theta = 130^\circ$.

2.3.4 STM

The STM is a powerful tool to image the surface structure based on the tunneling effect. When two conductors are brought close enough and a potential V applied between them, the overlap of the electron wavefunction permits quantum mechanical tunneling and a current I will flow across the gap.³⁰ During the operation, a conducting metal tip is scanned mechanically across the sample surface and the generated tunneling current is detected and recorded to form a continuous image of the surface. I is a function of tip position, applied voltage, and the local density of states (LDOS) of the sample. The tip sharpness, sample cleanness and environmental vibration condition are also key factors to obtain a good STM image.

There are two different operation modes of STM.³⁰ When performing the test in constant current mode, the tip is first brought close enough to the surface so that a tunneling current is measurable with a convenient operating voltage. A feedback network changes the distance d between the tip and the sample surface to maintain the constant current when the tip is scanned. Because the current is direct proportional to the distance, the tip is scanning the surface at the constant height over each atom. Thus a plot of the tip's relative position z versus x and y coordinates is a set of contours of the surface. When carrying the experiment in constant height mode, a tip is scanned across the surface at constant height and constant voltage. The feedback network responds to the changing current and the I is plotted versus x and y coordinates. Figure 2.8 illustrates these two scanning modes in STM.

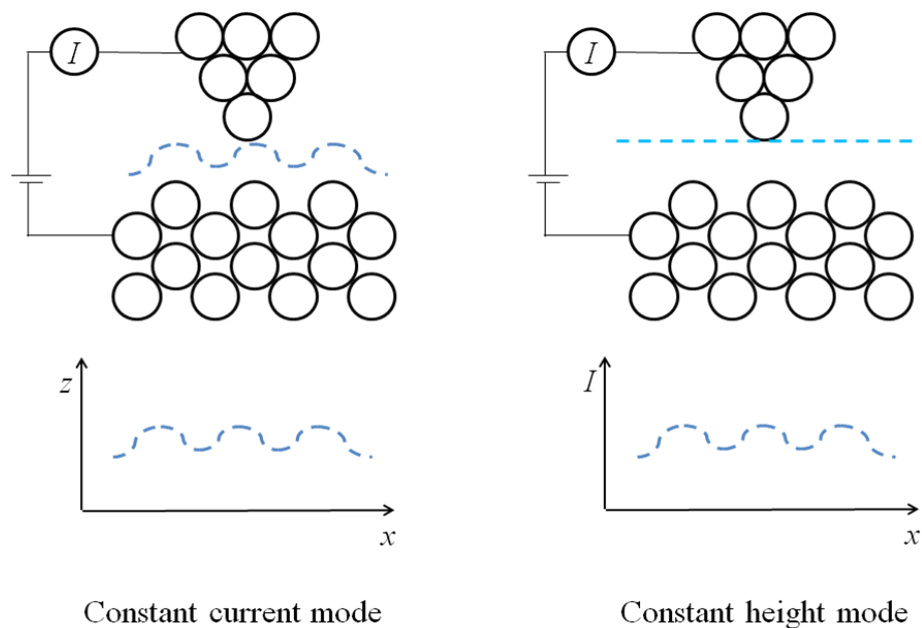


Figure 2.8 Scanning modes for STM, adapted from ref 30.

In our experiments, the images were generated under constant current mode in which the z direction distance is plotted directly and the bright color represents shorter distance between certain species and the tip or higher LDOS. The conducting tip was made by electrochemically etching the tungsten wire in NaOH or KOH solution. Tip sharpness was examined by microscope before transferring the tip into the UHV chamber. To minimize the vibration noise from the outside, all ion pumps, dry pump, turbo pump, ion gauges associated with the system were turned off and the sample was allowed to reach the thermal equilibrium with the scan stage before taking any images. A typical sequence of performing a STM scan is as follows: Pretreated sample was first transferred onto the STM scan stage and the correct connection between sample holder and scan stage was made sure. Turn off unnecessary electronics and pumps as mentioned above and set air

legs to floating position. Gently lower down the STM tip and keep a watch on the legs of tip holder to reach the sample holder ramp. Turn on the STM control electronics and set up for the tip approaching. Monitor the tip position through the CCD camera when the tip is getting close to the sample. If the tip is too long, it may crush the surface before the tip holder reaches the sample holder ramp. If the tip is too short, it may not be close enough to the surface at the end of ramp. In either case, the tip should not be used and must be adjusted after being taken out of UHV chamber. After the tip is successfully settled on the surface with a measurable tunneling current, let the system stay still for at least 10 min. Then check the vibration noise level and make the according changes to optimize the condition. It is now ready to take images.

Chapter 3 Structure of the Clean Pt (110) Single Crystal Surface

3.1 Introduction

The structure of clean Pt(110) single crystal surface has been extensively studied during the 1980's.^{25,26,33-38} There are several reconstructions found for this crystal, such as (1×2), (1×3), (1×5). The transition from (1×1) to (1×2) is kinetically irreversible²⁶. The rough surface created by ion bombardment at room temperature exhibited (1×1) phase. When the crystal was heated to 1130 ± 30 K the metastable (1×1) phase also appeared.³³ If the crystal is heated to 800 K under vacuum the metastable (1×1) phase will convert to stable (1×2) phase rapidly. Heat treatments in oxygen (> 1100 K) resulted in the appearance of (1×3), (1×5) and (1×7) surface structures while oxygen remains undetectable by AES.³³ Those types of reconstruction were also stable once created.

The structure of Pt(110)-(1×2) surface reconstruction was analyzed by low energy alkali impact collision ion scattering spectroscopy (ALICISS) which allows a direct correlation with the atom positions in real space. It was confirmed that only missing row (MR) model was consistent with all experimental data. In MR model, the structure could be described by long atom rows in the $\langle 1\bar{1}0 \rangle$ azimuth and on the average every second $\langle 110 \rangle$ row is missing, with some disorder occurring in the 1×2 periodicity.³⁶ The MR reconstruction model of Pt(110)-(1×2) surface is illustrated in Figure 3.1.³⁹ The unit cell is (0.277 × 0.784) nm. The depth of missing row is 0.277 nm and step height is 0.139 nm.

The objective of studying the clean Pt(110) surface is to establish the standard of our UHV-STM system and to provide the correction factor for future study.

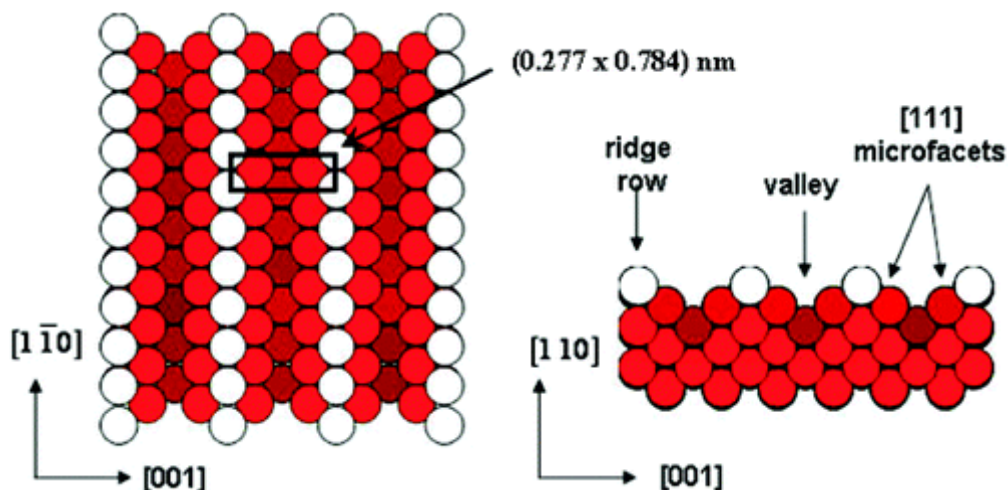


Figure 3.1 Structure of the clean Pt(110)-(1 \times 2) missing row reconstruction.

3.2 Experimental Methods

The Pt(110) single crystal used for this work had a diameter of 10 mm and a thickness of 1.5 mm. The sample was mounted to the commercial RHK sample holder, see Figure 2.3. A pair of chromel-alumel thermocouple wires was spot-welded to the side of crystal in order to measure the temperature and provide the ground connection when necessary.

The Pt(110) single crystal was cleaned using cycles of 500 - 1000-eV Ar⁺ ion sputtering followed by annealing at 600 K in $\sim 5 \times 10^{-8}$ Torr O₂. Ar⁺ Pressure varied from 1×10^{-5} to 1×10^{-4} torr. Depending on the amount of residue need to be cleaned, the sputtering time can vary from 10 min to several hours. Heating to higher temperature under O₂ environment caused the formation of (1 \times 3) reconstruction which is quite stable and can only be eliminated by sputtering. So radiation heating is enough for O₂ treatment. After this step, the crystal was annealed to 1200 K for 30 sec in vacuum by e-beam

heating method. The bias applied between the sample and the filament was up to 500 V. The sample cleanliness and orderliness were tested by XPS, AES and LEED. Once confirmed, the sample was moved to STM scanning chamber and performed the final cycle of O₂ treatment and high temperature annealing. The sample was then transferred to STM scan stage and ready for STM image after cooling to room temperature.

STM imaging was carried using constant current mode. The general operation parameters were: tunneling current 0.4 ~ 0.8 nA, bias $\pm 0.1 \sim 2$ V, scan rate 50 $\mu\text{m/s}$. But one can change them when necessary. Detailed information will be given under each image.

3.3 Results and Discussion

The STM images of clean Pt(110) single crystal surface are shown in Figure 3.2 A and B. It was found that after high temperature annealing in vacuum, the surface was dominated by (1 \times 2) MR reconstruction structure. Mismatches such as (1 \times 3) reconstruction and defects were observed at the end of terraces. The plotting of line corrugation in Figure 3.2 C shows that the direct measured step height is about 0.1 nm, the depth of (1 \times 3) valley is 30 ~ 38 pm, the depth for (1 \times 2) valley is only about 10 pm. The distance between each ridge row for (1 \times 2) reconstruction is about 0.8 nm, which is ~ 1.2 nm for (1 \times 3) reconstruction.

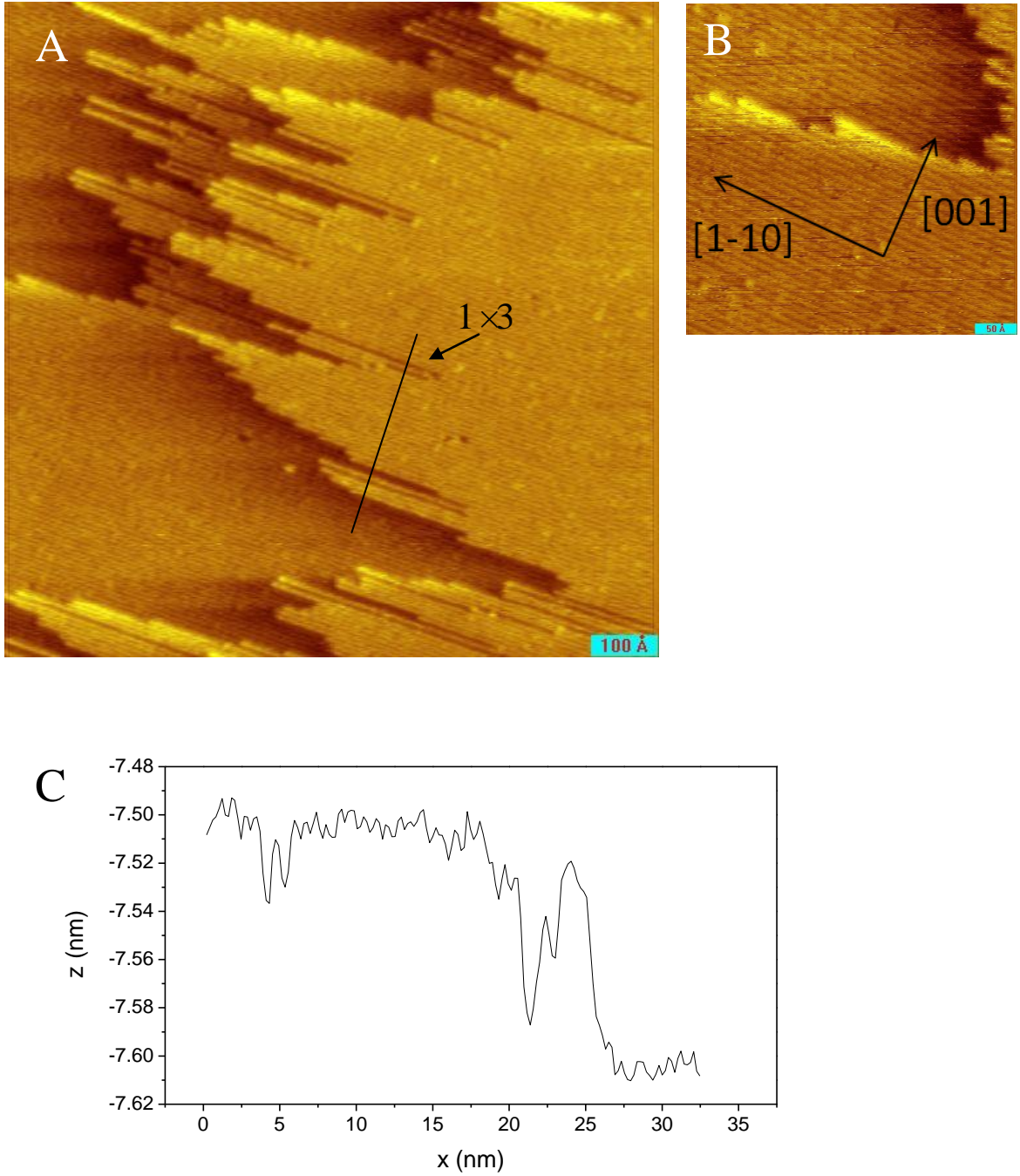


Figure 3.2 A and B: Clean Pt(110) surface with the (1×2) missing-row reconstruction. STM images were taken at room temperature, $I = 0.79 \text{ nA}$, $V = -142 \text{ mV}$. Image size: $(1000 \text{ \AA} \times 1000 \text{ \AA})$ and $(400 \text{ \AA} \times 400 \text{ \AA})$. C: Cross-sectional view of the black line in A.

These results first confirms our ability of making clean and ordered Pt(110)-(1×2) surface. Comparing our measured distances and depths with Pt(110) lattice constant, it is also confirmed that the measurement on x and y coordination is accurate while the reading on z direction is off by 1.7. The correction is tabulated in Table 3.1 in which the distances from STM images were calculated by statistically counting 6 ~ 10 distances for each kind and given in form of the average ± standard derivation.

Table 3.1 Comparison of distances obtained directly from STM images and from a lattice model

Distances from		STM images (nm)	Lattice model (nm)	% error	correction coefficient
x, y direction	(1×2) row distance	0.802 ±0.052	0.784	8.9	0.98 ≈ 1
	(1×3) row distance	1.151 ±0.040	1.176	5.5	1.02 ≈ 1
z direction	step height	0.082 ±0.004	0.139	41.0	1.7

3.4 Conclusions

The results of clean Pt(110) crystal surface obtained in our chamber were consistent with that from the previous publications, in which a (1×2) missing row reconstruction is the most stable phase and Pt atoms are close packed along [110] direction. It is proved that we have the capability of studying the Sn- Pt(110) bimetallic surfaces.

Chapter 4 Structure of Sn/Pt(110) Surfaces with Medium Sn Coverage

4.1 Introduction

As mention in Introduction section, up to now, there is only one publication reported the structure study of depositing Sn on to Pt(110)-(1×2) surface.²³ It is said that adding 0.4 ML Sn to clean Pt(110) caused formation of three different configurations at room temperature: alloyed Pt–Sn–Pt chains (C in Figure 4.1) and mobile Sn ad-atoms in the valley of the missing row reconstruction (B in Figure 4.1), and small 3D Pt–Sn alloy islands (A in Figure 4.1). The islands formed before the valleys were completely filled and the alloyed Pt-Sn-Pt chains were not detected by LEED.

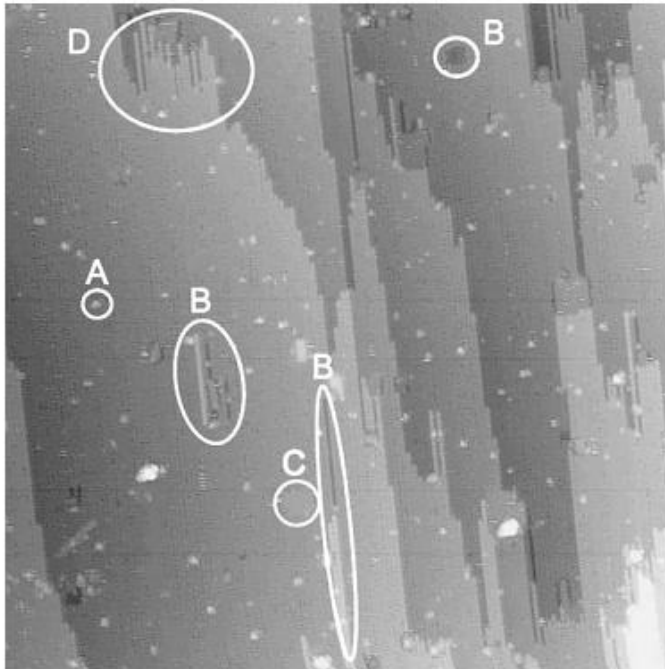


Figure 4.1 STM image of Pt(110)-Sn surface at 0.4 ML Sn coverage, adapted from ref. 23.

4.2 Experimental Methods

The same sample and sample clean procedure as described on last chapter were carried here.

Deposition of Sn was accomplished through a homemade Sn doser. The Sn doser was built using a 2-conductor, high-voltage, electrical feed-through mounted on a 2.75-in Conflat™ flange. A resistively heated Ta “boat” containing high purity Sn (6N) was suspended between two 0.010-in Ta wires that were spot-welded to the Cu feed-throughs. The diameter of the pinhole in the Ta sheet covering the Ta-boat was 0.5 mm. A stainless steel foil shield and tube were attached to one of the Cu rods and positioned directly above the pinhole to restrict the path of Sn to the sample region. The boat was heated resistively using a DC power supply.

Sn coverage was monitored by XPS, AES and LEIS. As-deposited sample was then annealed gradually to 1200 K to monitor the Sn-Pt interaction and STM imaging was carried when the sample was annealed to 750 K and 1000 K.

4.3 Results and Discussion

4.3.1 Determination of the Sn coverage

Initially we tried to identify the ML coverage of Sn by LEIS. A typical LEIS uptake curve is shown in Figure 4.2. It is obvious that the clean Pt(110) surface exhibited only one Pt peak at 930 eV. Right after the first Sn dosing, the Sn peak grew to as large as the Pt peak. Repeating the same Sn dosing procedure for four times, the complete cover of Sn signal over the Pt signal did not appear. Instead the Sn: Pt value was always around

0.5~ 0.7 means the surface was covered approximately half Sn and half Pt. But the Sn/Pt XPS peak area ratio obtained from the 100 sec deposition sample is 0.33, which means over 1 ML Sn had been deposited on the surface. This is the evidence that the deposition of Sn on Pt(110) surface doesn't follow the layer-by-layer model and it is possible that either room temperature alloying occurred or Sn was accumulated as big clusters. Hence the LEIS is not suitable for determining Sn coverage in Sn-Pt(110) system.

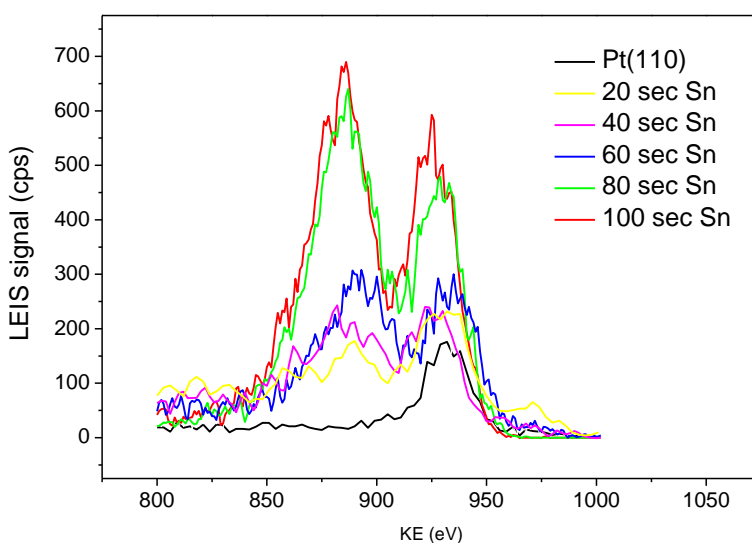


Figure 4.2 LEIS spectra of Sn-deposited Pt(110) surface with increased Sn exposure

After cleaning out the sample, another uptake experiment was performed using XPS and AES. Results are shown in Figure 4.3. The Sn XPS signal grew in three different regions and the first break point corresponding to a Sn/Pt XPS ratio of 0.18. That is very close to what is found to be 1 ML of Sn on Pt(111). Thus this break point is assigned to be the 1 ML of Sn on Pt(110) surface. Due to the cumulated carbon contamination during

the measurements, AES uptake curve had a lot irrational jumping data point and is not shown in this thesis.

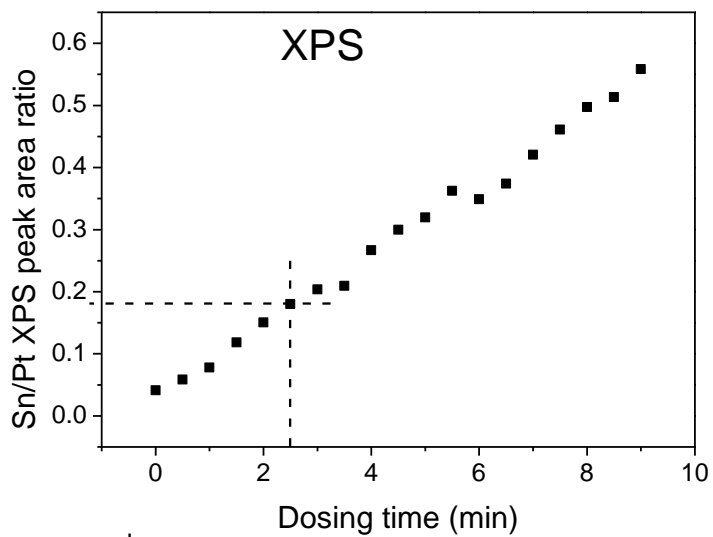
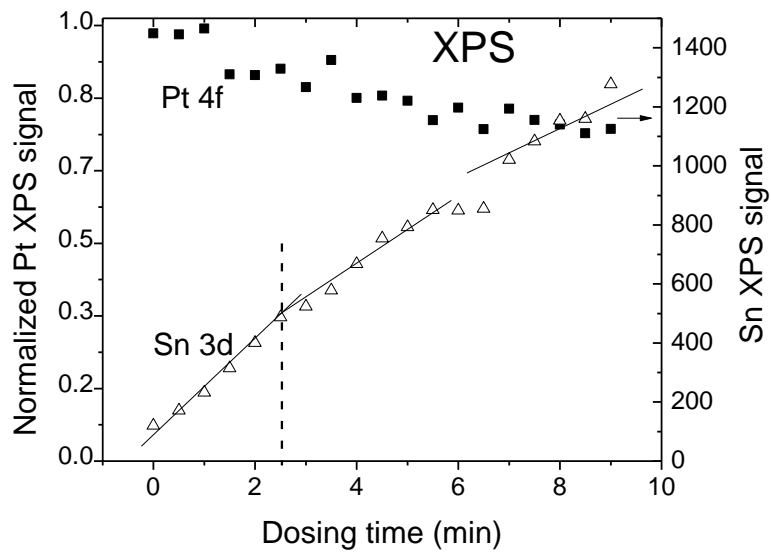


Figure 4.3 XPS uptake curves for Sn deposited on a Pt(110) surface.

4.3.2 Temperature Influence on Surface Composition

After deposit ~ 1 ML of Sn on pre-cleaned Pt(110) surface, the sample was gradually annealed to 1200 K and the change of surface Sn concentration was shown in Figure 4.4.

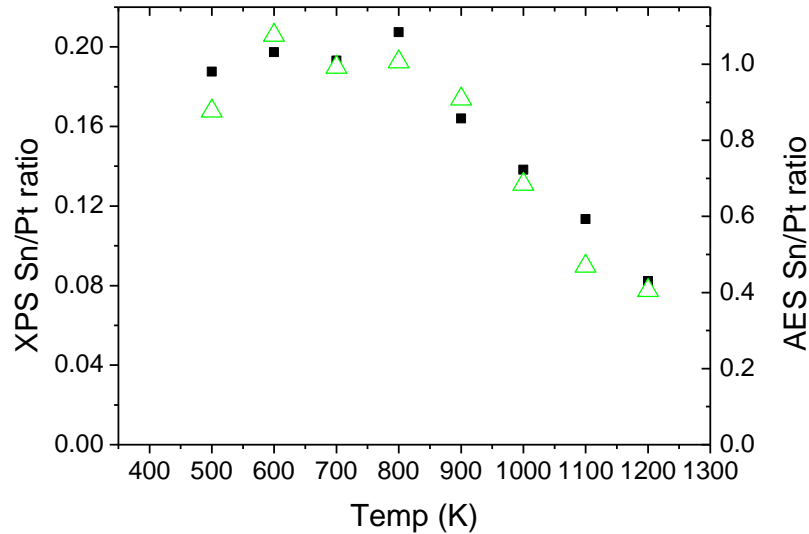


Figure 4.4 Surface Sn concentration varies with annealing temperature. The black solid square represents the Sn/Pt XPS peak area ratio; the green hollow triangle indicates the Sn/Pt AES peak height ratio.

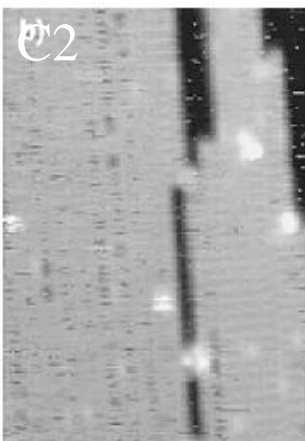
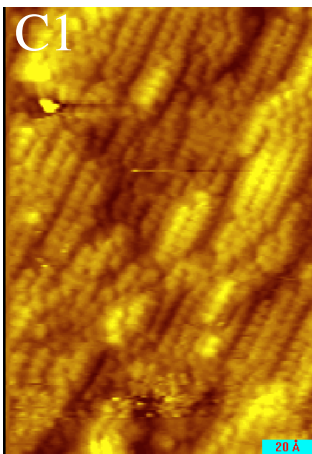
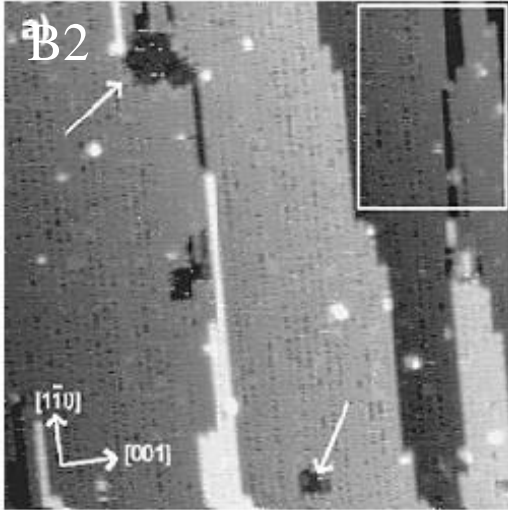
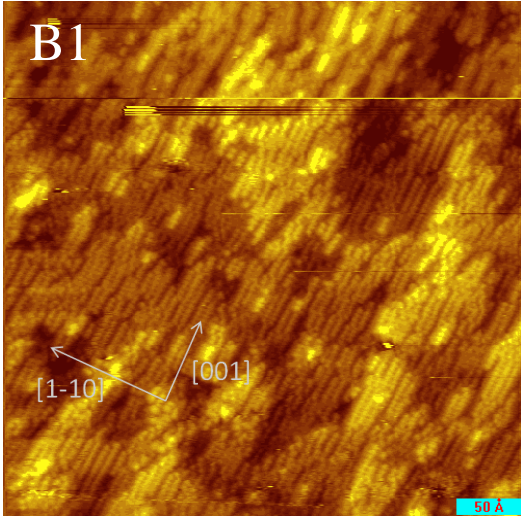
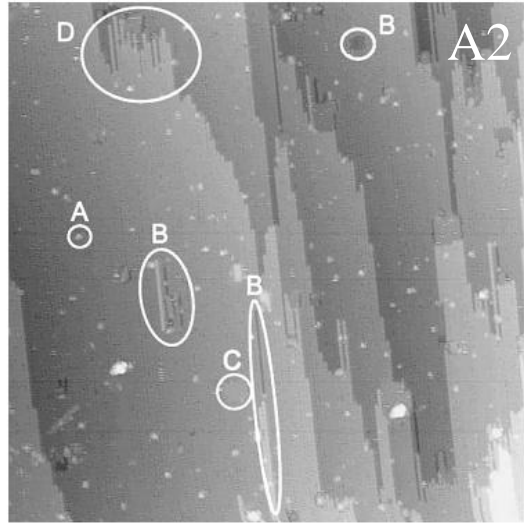
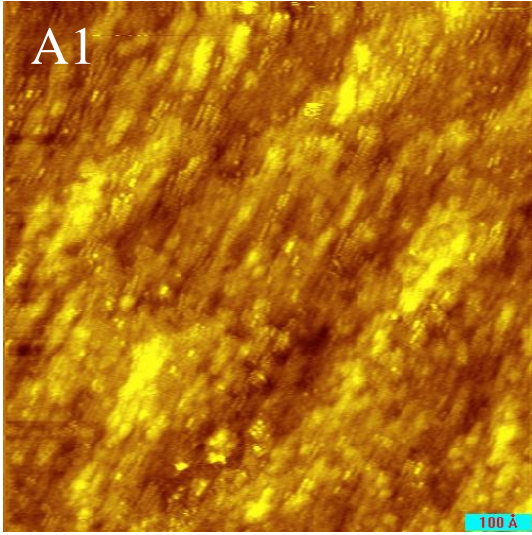
The temperature influences examined by both XPS and AES agreed with each other as shown clearly in Figure 4.4. Sn started to dissolve into bulk Pt crystal when annealing at 900 K. At 1200 K, the surface Sn is less than 50% of the initial concentration. But for samples at all temperatures, including the as-deposited room temperature one, the LEED results remained as weak (1×1), no distinct pattern was observed. Therefore, STM imaging was only performed on samples at two stages of annealing, 750 K and 1000 K.

4.3.3 STM Results

The sample used in this section contained 1 ML of Sn with Sn/Pt XPS ratio = 0.184 and is denoted as 1-ML Sn/Pt(110). STM images with various scales of the 1-ML Sn/Pt(110) sample followed with annealing to 750 K for 3min are shown in the left panel of Figure 4.5. The right panel is displaying the results from Janin's research²³ of 0.4 ML Sn on Pt(110) in the same scales for comparison.

When annealed to 750 K, Pt(110) surface remained its (1×2) MR reconstruction feature after small amount of Sn being deposited. However, the surface of 1-ML Sn/Pt(110) had no hint of the original structures at all. The bright balls in Figure 4.5 C1 and D1 are assigned as Pt atoms. Since the LDOS of Pt is higher than Sn, Sn atoms tend to form dark spots when imaging with Pt. It is observed that the (2×2) Pt-Sn-Pt alloy chain is the dominant species on this surface. But their regularity was quite short. Chains ended every 20 or less Pt atoms, while large amount of steps and mismatches co-existed on the surface. This can also explain the lack of (2×2) pattern from LEED.

When annealed to 1000 K, 0.4-ML Sn/Pt(110) surface lost its flat terraces and became more disordered than lower temperature annealing. (2×2) Pt-Sn-Pt alloy was also not detectable. The 1-ML Sn/Pt(110) surface, as shown in Figure 4.6 A, on the opposite, became flatter although only (1×1) LEED pattern was observed. The surface was revealed to have larger terraces rather than the short chains shown in Figure 4.5 But the long term orderliness was still not enough to generate the diffraction pattern.



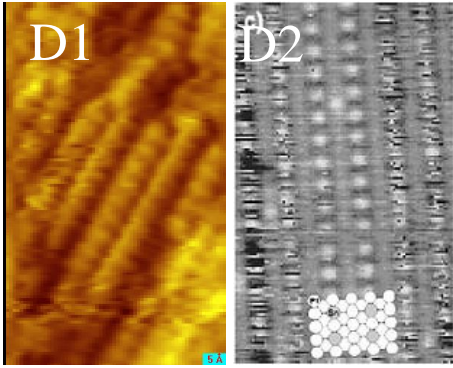


Figure 4.5 STM images of 1-ML Sn/Pt(110) surface annealed to 750 K for 3 min. (A1)(A2) 100 nm \times 100 nm, (B1) (B2) 40 nm \times 40 nm, (C1)(C2) 12 nm \times 17 nm, and (D1)(D2) 4.5 nm \times 8 nm.

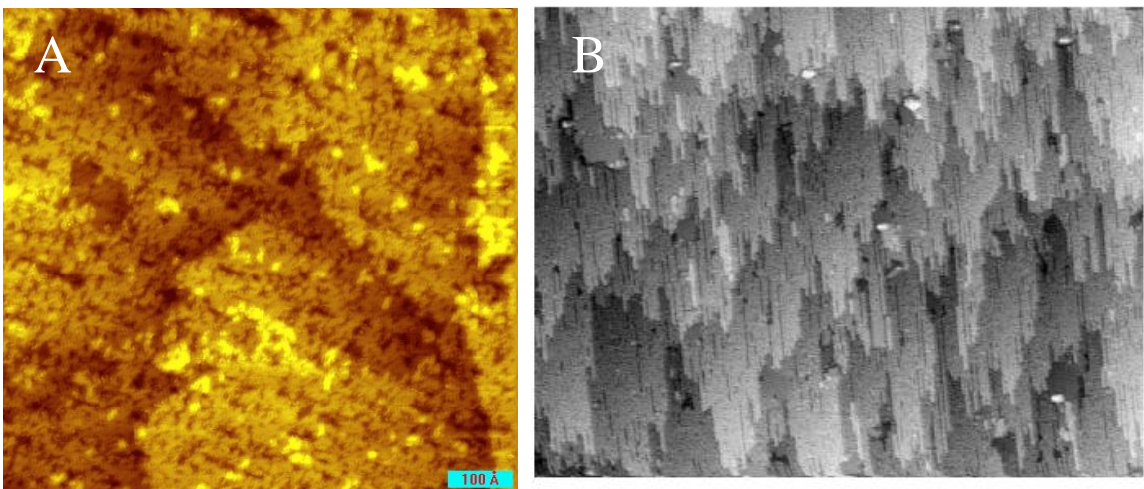


Figure 4.6 STM images of 1-ML Sn/Pt(110) annealed to 1000 K for 3 min. (A) 80 nm \times 80 nm, (B) 13.2 nm \times 10.2 nm²³.

4.4 Conclusions

Sn evaporated on to a clean Pt(110)-(1 × 2) crystal sample alloyed with the substrate Pt at room temperature. Sn film growth on Pt(110) did not obey the S-K mode therefore the LEIS is not suitable to determine the film thickness.

Deposition of 1 ML of Sn changed surface morphology differently than that of 0.4 ML Sn exposure. The short-range (2 × 2) Pt-Sn-Pt alloy chains along the [001] direction dominated the surface when annealing at 750 K for 3 min. Annealing to 1000 K flattened the surface a little bit, which still contained abundant defects and mismatches. In both cases, only (1 × 1) LEED pattern was observed.

Annealing the sample of 1-ML Sn/Pt(110)-(1 × 2) to higher temperature also led to a loss of Sn from near surface region. Sn started to dissolve into bulk from 800 K. After annealing to 1200 K, only 45% of the original Sn was detected by XPS.

Chapter 5 Structure of Sn/Pt(110) Surfaces with High Sn Coverage

5.1 Introduction

For the other transition metal studied on Pt(110) surface, such Co¹⁶⁻¹⁸, Ni^{19, 20}, *etc.*, it is always noticed that 1 ML of the second element is not enough to cover the Pt(110) surface. Since the first 0.5 ML would be used to fill the missing rows, approximately 1.5 ML is more adequate to fully cover the substrate lattice.

As mentioned before, at the low Sn coverage (0.4 ML) from Janin's literature,²³ the Pt(110)-(1×2) surface was barely affected with only small amount (2×2) alloy and 3-dimensional island were observed. Our research about 1 ML Sn on Pt(110) presented in Chapter 4 of this thesis can only prove that the room temperature alloying occurred rapidly and substrate started to have significant change in morphology. LEIS showed that for our so called 1 ML Sn/Pt(110), there was still 50% Pt signal detectable. Therefore a set of experiment for samples with $\theta(\text{Sn})$ greater than 1.5 ML is required.

5.2 Experimental Details

The same sample and cleaning procedure as described in previous chapters of this thesis were carried out. Sn dosing was performed from the same homemade Sn doser, only heating condition was slight turned up. Two sets of experiment were performed, one with sample containing Sn/Pt = 0.49, $\theta(\text{Sn}) = 2.7$ ML, and the other had the values of Sn/Pt = 0.35, $\theta(\text{Sn}) = 1.9$ ML. It is found that two samples showed identical LEED pattern evolution during annealing, which means the alloy process is reproducible and

followed a certain path. For convenience, only the first sample will be discussed and is denoted as 2.7-ML Sn/Pt(110) in results section below

5.3 Results and Discussion

5.3.1 Temperature Influence on Surface Composition

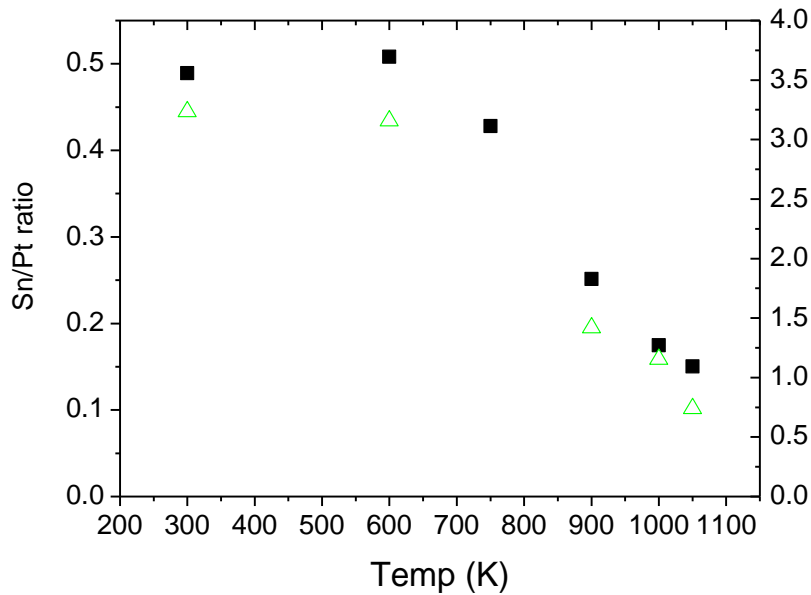


Figure 5.1 Surface Sn concentration varies with annealing temperature. The black solid square represents the Sn/Pt XPS peak area ratio; the green hollow triangle indicates the Sn/Pt AES peak height ratio.

Compared with Figure 4.4, the XPS/AES ratio versus annealing temperature for 1-ML Sn/Pt(110), Figure 5.1 demonstrates the similar trend that Sn stayed at the near surface region the sample was not too hot. Sn would start to dissolve into bulk Pt(110) crystal when T was greater than 700K. The onset dissolving temperature decreased from

800 K to 700 K, which may be explained by the lower binding ability between Sn and Pt at high Sn coverage.

5.3.2 LEED Results

Not only the surface composition but also the surface structures were changed during the annealing of 2.7-ML Sn/Pt(110) sample. The structural changes were captured by LEED and new patterns are shown in Figure 5.2

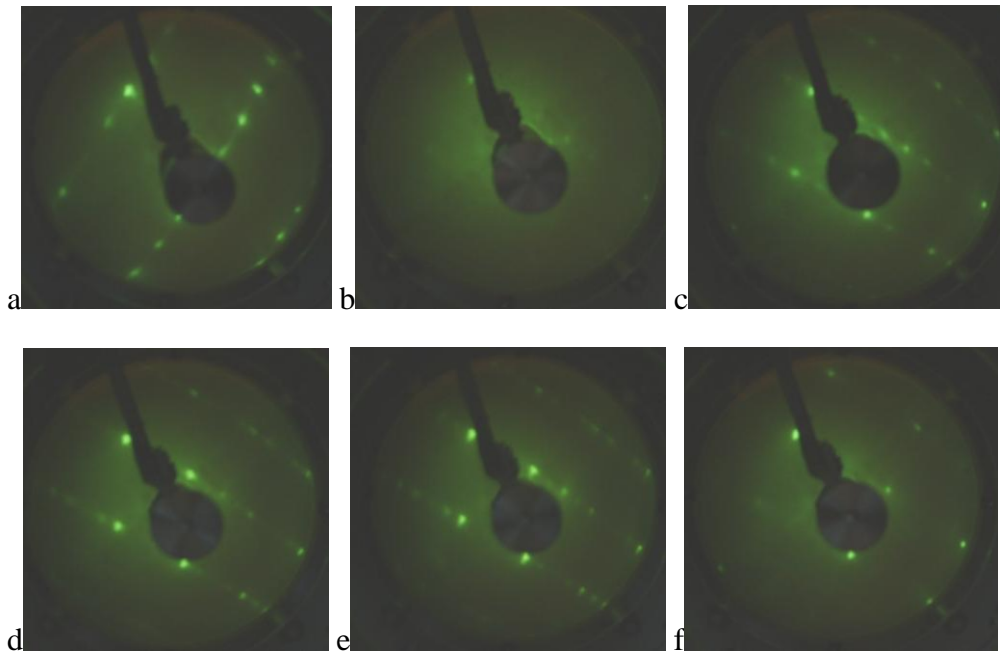


Figure 5.2 LEED pattern evolution of Sn alloying process. (a) clean Pt(110)- (1×2) ; After depositing 2.7 ML Sn, (b) room temperature, anneal to (c) 600 K, (d) 750 K, (e) 900 K, (f) 1050 K.

Distinct LEED patterns were observed when gradually anneal the 2.7-ML Sn/Pt(110) to different temperature. The LEED pattern developed from (1×2) to (4×1) to

(6×1) and finally (1×1), which are shown in Figure 5.2. The identical evolution path was also observed for depositing 1.9 ML Sn on to clean Pt(110)-(1×2) surface. This indicates that there are multiple structures involved in the Pt-Sn alloy process. And STM imaging under each transition temperature is required to reveal them.

5.3.3 STM Results

In order to discover the alloying pathway and intermediates associated with the four distinguished LEED patterns, STM experiment was carried for 2.7-ML Sn/Pt(110) sample at six stage, as-deposited, annealing to 600 K, 700 K, 900 K, 1000 K and 1050 K. The results are shown in following figures.

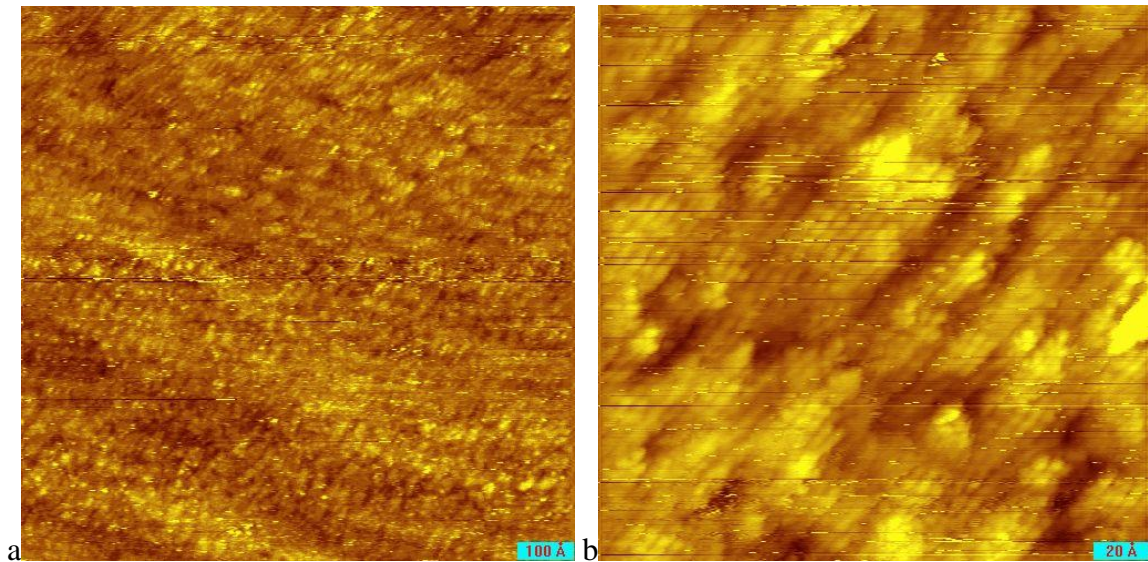


Figure 5.3 STM images of 2.7-ML Sn/Pt (110), as-deposited. No annealing. Images are (1000 Å × 1000 Å) (200 Å × 200 Å) large, taken under -160 mV, 0.56 nA and -252 mV, 0.56 nA, respectively.

It is clear that right after the Sn was deposited, the substrate missing row structure disappeared. It might be covered underneath the Sn film or dismissed by alloying with Sn. This 2.7 ML Sn deposition corresponds to a Sn/Pt XPS peak area ratio of 0.49. The same amount Sn deposition performed on Pt(111) sample showed an LEIS peak ratio of Sn/Pt = 88:12. So it is reasonable to assign the visible atom these two images as Sn. Sn atoms are now packed along [001] direction. Row distance was about 5 Å. Corresponding LEED pattern is Figure 5.2 (b).

The surface started to have more features when annealed to 600 K as its LEED pattern showed a weak (4×1), see Figure 5.2 (c). STM results with various scales of 2.7-ML Sn/Pt(110) surface annealed to 600 K are shown in Figure 5.4. Careful examination tells that the dark row distance indicated by black arrows (arrow 1, 2, 3) is 11.3 Å, which is about four times of 2.77 Å. Atom-to-atom distance along the [001] row is 4 Å, which matches the (1×1)-Pt(110) lattice distance, 3.92 Å. Thus, this image confirms the (4×1) LEED pattern. Magnified scan showed in the last image Figure 5.4 (d) suggests a tri-atomic strip. But the third atom is a little off-plane, which gives the darker color and looks like the valley in the previous image (c). At this temperature, the Sn/Pt XPS ratio did not change much comparing to the as-deposited one. Therefore, the surface is dominated by Sn atoms.

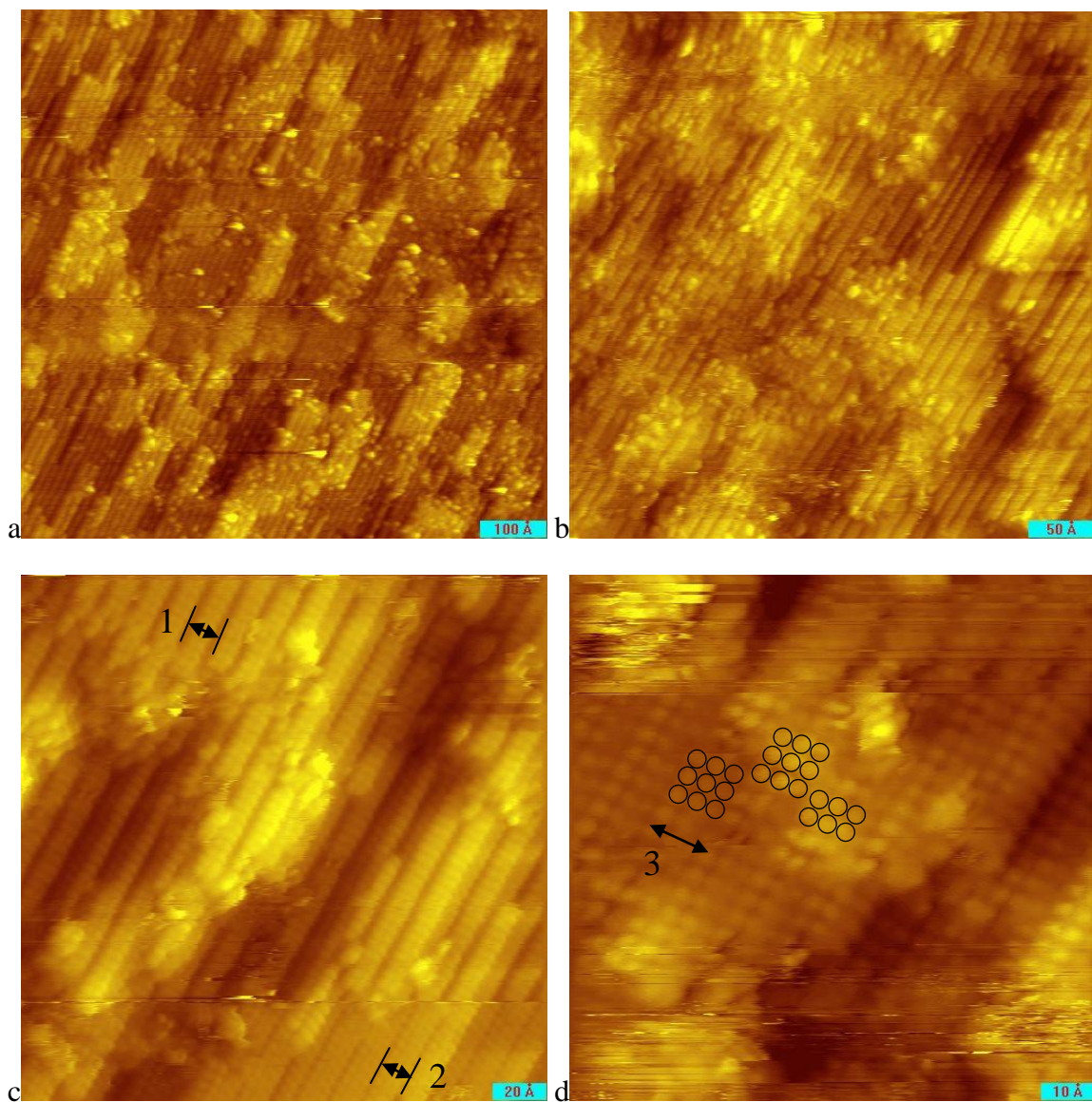


Figure 5.4 STM images of 2.7-ML Sn/Pt (110) after annealed to 600 K. Images are (1300 Å × 1300 Å) -1.07 V, 0.56 nA, (400 Å × 400 Å) 0.90 V, 0.56 nA, (200 Å × 200 Å) -85.3 mV, 0.56 nA, and (100 Å × 100 Å) -7.82 mV, 0.56 nA, respectively.

Another interesting point is that arrow 1 and 2 in Figure 5.4 (c) seemed to represent different structures. Two continuous scans of the same region shown in Figure 5.5 demonstrated that they were reversible and probably belonged to the same structure.

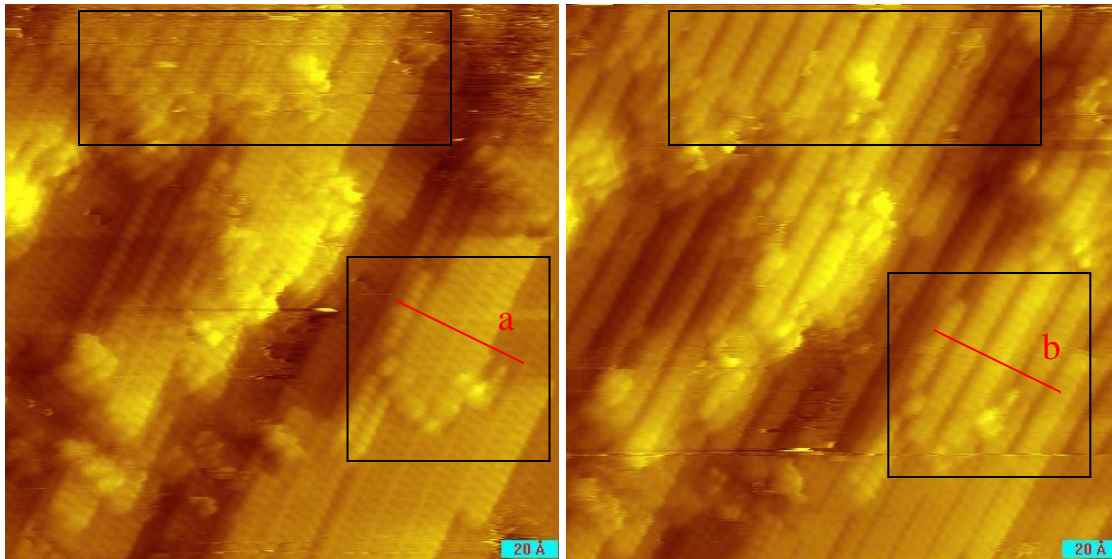


Figure 5.5 STM images of 2.7-ML Sn/Pt (110) after annealed to 600 K. These two images were taken continuously of the same spot without changing tunneling current and scan voltage, both are $(200 \text{ \AA} \times 200 \text{ \AA})$ -85.3 mV, 0.56 nA.

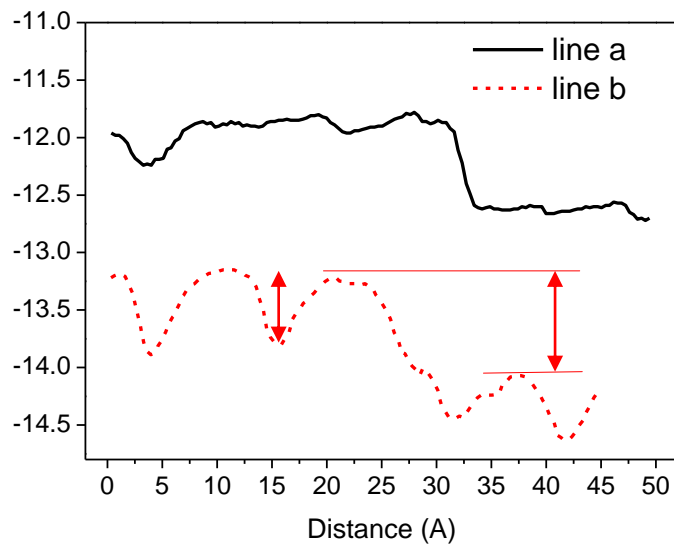


Figure 5.6 Cross-sectional view of line a and b in Figure 5.5. The distance unit is \AA . The step size is 0.8 \AA and the valley depth in line b is 0.5 \AA , measured from images directly without correction. After correction, the valley depth should be 0.85 \AA .

It is clear that the third atom in the tri-atomic strip is more visible in Figure 5.5 (a) than in the Figure 5.5 (b). But it is hard to believe all the atoms in the third rows have moved simultaneously to deeper layer within in room temperature. The difference here is more likely due to some electronic effect.

Anneal to 600 K, Sn atoms packed as tri-atomic strips growing along [001] direction (Figure 5.4 ~ 5.6). With annealing temperature increasing, surface Sn/Pt ratio kept decreasing, which may be due to the dissolution of Sn into bulk. At **700 K**, the Sn/Pt ratio was 85% of the initial value and tri-atomic strips still dominated the surface (Figure 5.1). Co-existing triangular prisms-like structures were also observed. (Figure 5.7 (b)(c)) It is possible that the hill atoms are Pt and they are forming (2×2) Pt-Sn alloy on the facets, which was indicated by the brightest spots on LEED pattern (Figure 5.2 (d)). But there is no solid evident for this faceting effect. It also becomes difficult to say which atoms are Pt and which are Sn. Since Pt should be brighter than Sn when imaging together, we will tentatively assign the visible balls as Pt atoms.

Atom-to-atom distance along the hill is also 4 Å. Ridge row to ridge row distance indicated by the black arrow in Figure 5.7 (b) is 17 Å, close to $6 \times 2.77 \text{ \AA} = 16.62 \text{ \AA}$, which explains the (6 × 1) LEED pattern raising in Figure 5.2 (d).

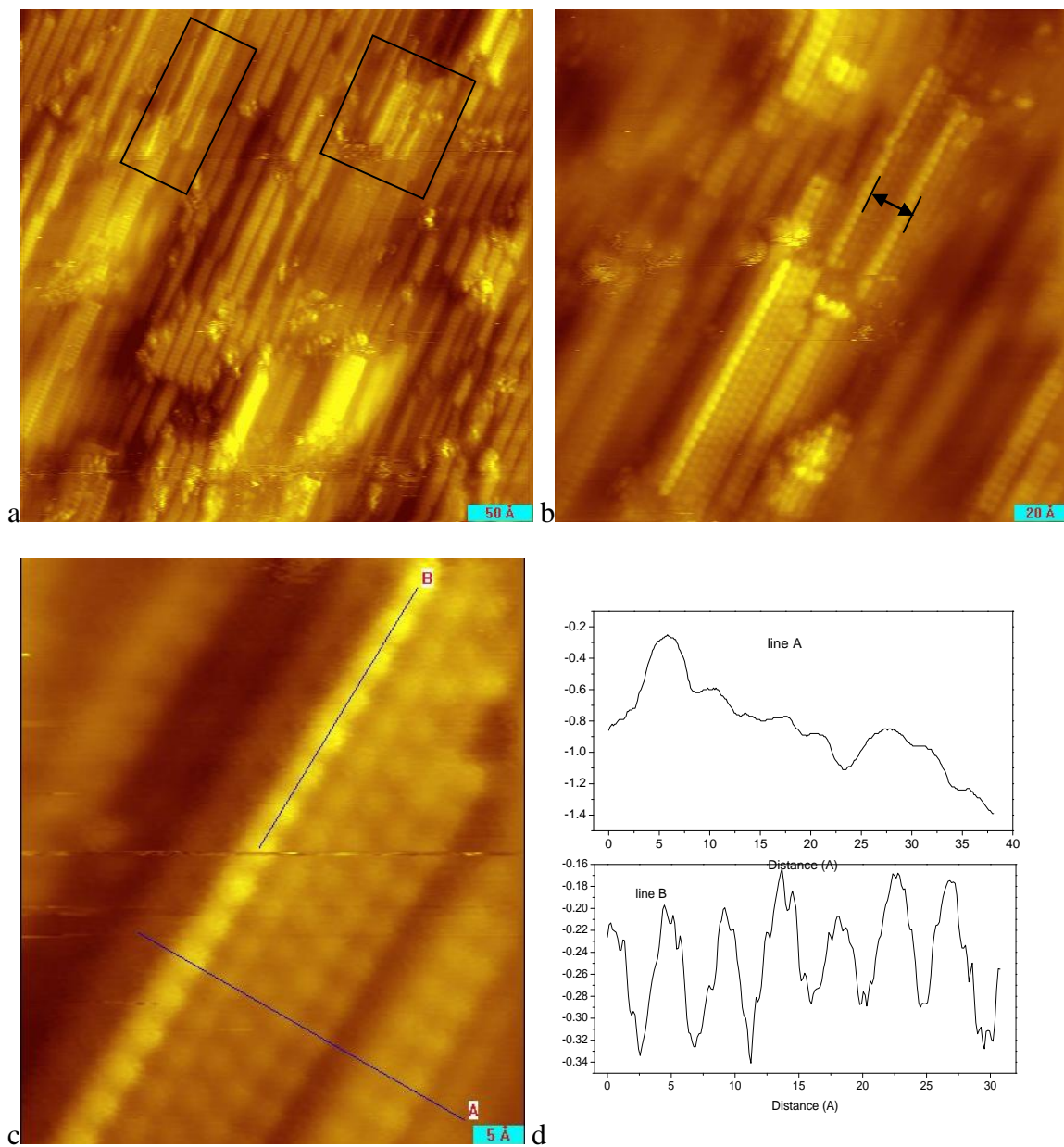


Figure 5.7 STM images of 2.7-ML Sn/Pt (110) after annealed to 700 K. Image (a) ($400 \text{ \AA} \times 400 \text{ \AA}$) -66.2 mV, 0.56 nA, shows the co-existence of tri-atomic strips and triangular prisms. Image (b) ($200 \text{ \AA} \times 200 \text{ \AA}$) -66.2 mV, 0.56 nA. Image (c) ($50.8 \text{ \AA} \times 59.4 \text{ \AA}$) -66.2 mV, 0.56 nA. (d) Cross-section of line A and line B in (c).

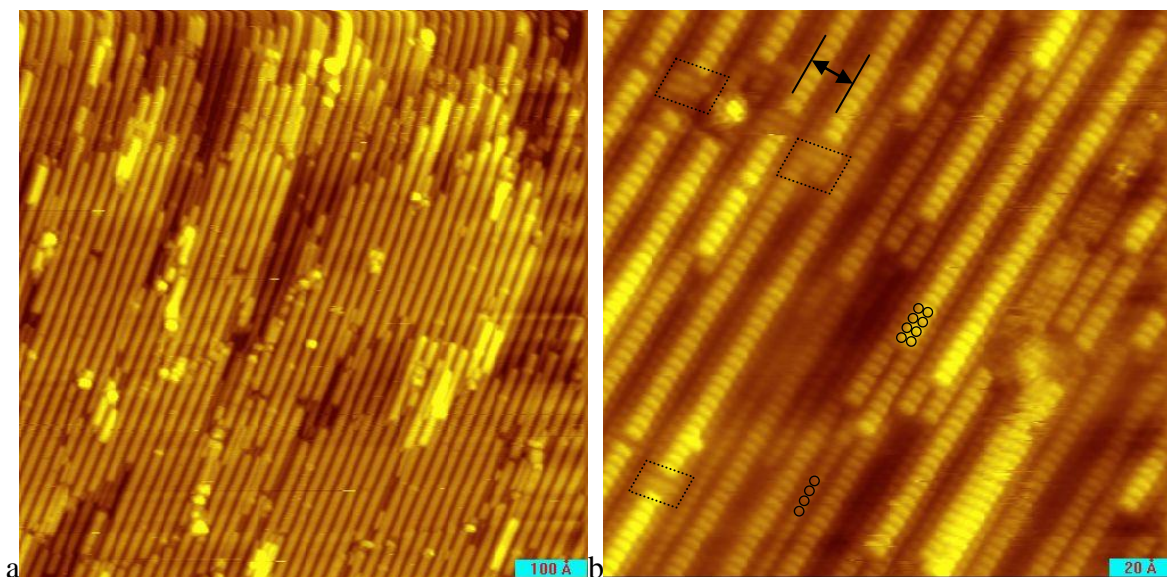


Figure 5.8 STM images of 2.7-ML Sn/Pt (110) after annealed to 900 K. Images are ($800 \text{ \AA} \times 800 \text{ \AA}$) and ($186 \text{ \AA} \times 186 \text{ \AA}$), taken under -131 mV , 0.81 nA and -9.73 mV , 0.67 nA , respectively.

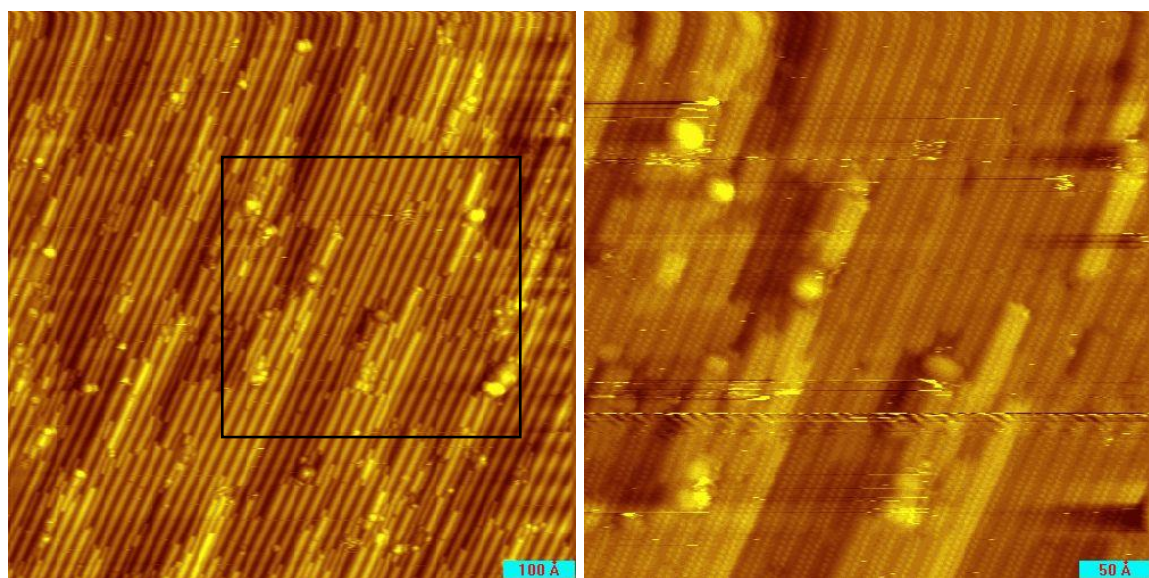


Figure 5.9 STM images of 2.7-ML Sn/Pt (110) after annealed to 900 K. Image (a) ($800 \text{ \AA} \times 800 \text{ \AA}$) -1.82 V , 479 pA , 14.5 \AA , (b) magnified scan of selected area, ($400 \text{ \AA} \times 400 \text{ \AA}$) -184 mV , 479 pA .

Instead of triangular prisms, after annealing at 900 K, the surface was flatter and consisted of ordered bi-atomic rows as shown in Figure 5.8. The row distance and atom-to-atom distance along the row matched (6×1) LEED pattern in Figure 5.2 (e). There are also some mismatches, such as holes, single-atom row and connected double rows (shown in dash-line squares). The second layer was more close-packed which corresponding to a (3×1) feature.

The images shown in Figure 5.9 were taken from the same sample condition as those shown in Figure 5.8. Two ($800\text{ \AA}\times 800\text{ \AA}$) pictures were almost identical, but you can see clearly the atomic level separation in Figure 5.9 (b), which confirms the bi-atomic row model.

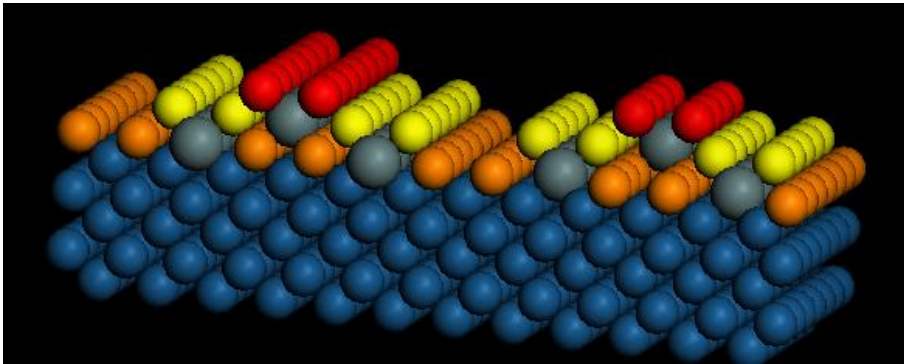


Figure 5.10 Possible model of 2.7-ML Sn/Pt(110) surface at 900 K. Grey balls are Sn atoms, all other colors are Pt atoms, red is the top layer, yellow is the second layer, orange is the third layer and blue is bulk Pt.

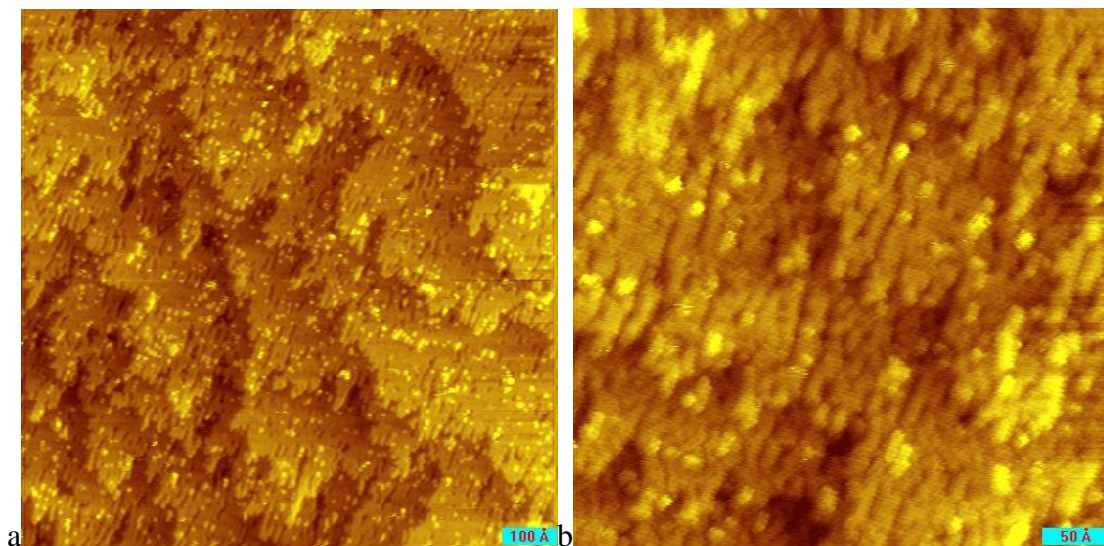


Figure 5.11 STM images of 2.7-ML Sn/Pt (110) after annealed to 1000 K. Images are ($1000 \text{ \AA} \times 1000 \text{ \AA}$) and ($400 \text{ \AA} \times 400 \text{ \AA}$), taken under 2.13 V, 0.70 nA and -73.0 mV, 0.59 nA, respectively.

After annealing to 1000 K, Sn/Pt ratio was only 40% of its initial value, the surface lost all the features along [001] direction. This group of images are actually comparable to the medium coverage of 1-ML Sn/Pt(110) at 1000 K, see Figure 4.6 A. Big terraces with lots of defects, adatoms and mismatches started to appear. Sample surface was too rough that we couldn't get better images.

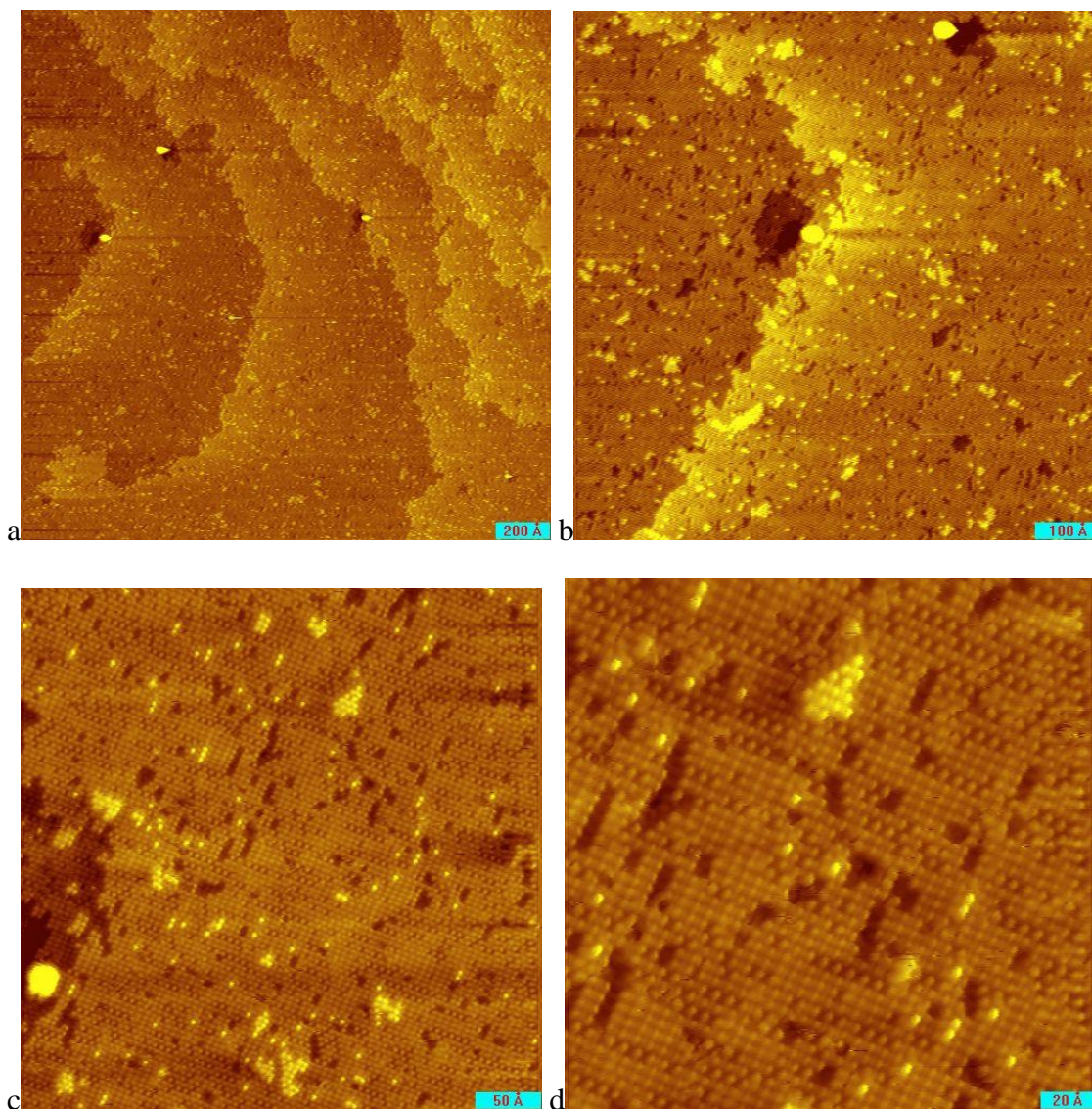


Figure 5.12 STM images of 2.7-ML Sn/Pt (110) after annealed to 1050 K. Images are (a) ($2000 \text{ \AA} \times 2000 \text{ \AA}$) 221 mV, 0.59 nA, (b) ($800 \text{ \AA} \times 800 \text{ \AA}$), (c) ($400 \text{ \AA} \times 400 \text{ \AA}$) and ($200 \text{ \AA} \times 200 \text{ \AA}$), respectively. (b-d) were taken under 406 mV, 0.59 nA,

This surface was now nice and flat, with great similarity to the $\text{Pt}_3\text{Sn}(110)$ bulk single crystal (See Figure 5.13). At the same time, Sn/Pt ratio is only 30% of its initial value, means most Sn deposited on the surface has either dissolved into bulk or

evaporated into gas phase after 1050 K annealing. We can then assign the visible atoms in above pictures as Pt. In [1-10] direction, Pt-Sn-Pt-Sn alloy chain was formed which should lead to a (2×1) LEED pattern. However the alloy chain is short-ranged and missing Sn or multiple Pt-Sn-Pt atoms occurred occasionally. Adatoms (monomer and dimer), holes and 2-dimensional islands co-existed with the ordered alloy surface. Therefore only (1×1) LEED was observed (Figure 5.2 (f)).

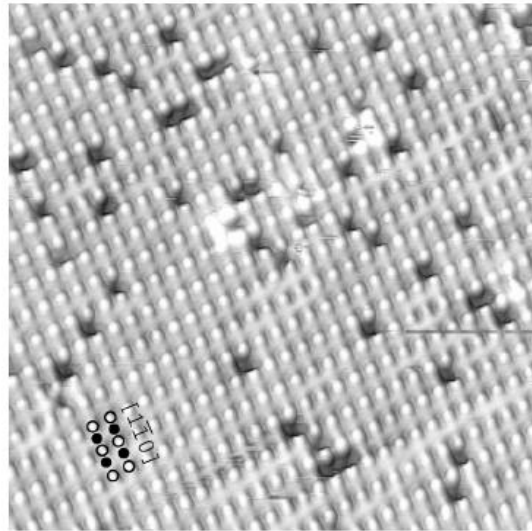
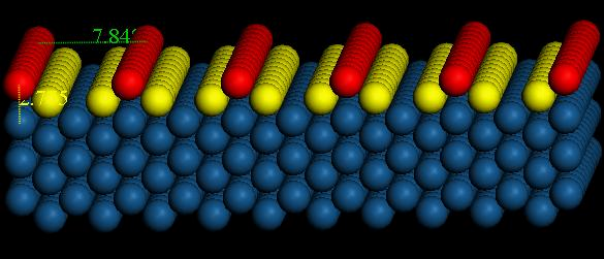
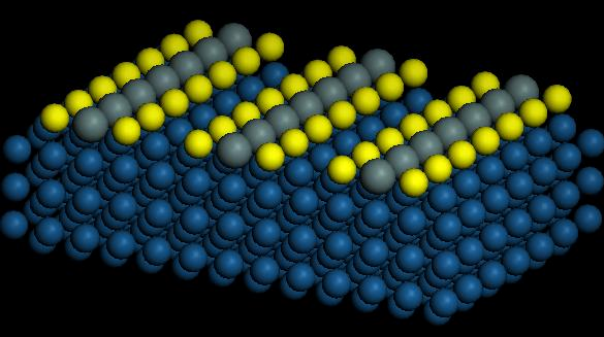
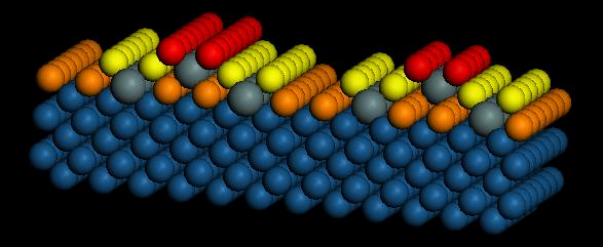
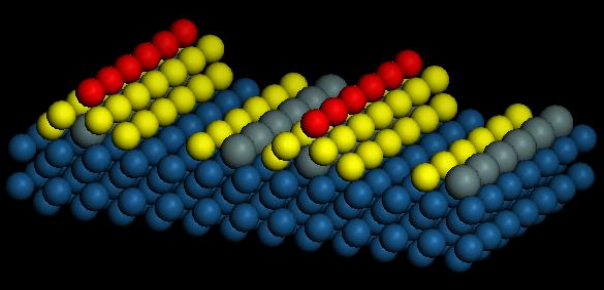
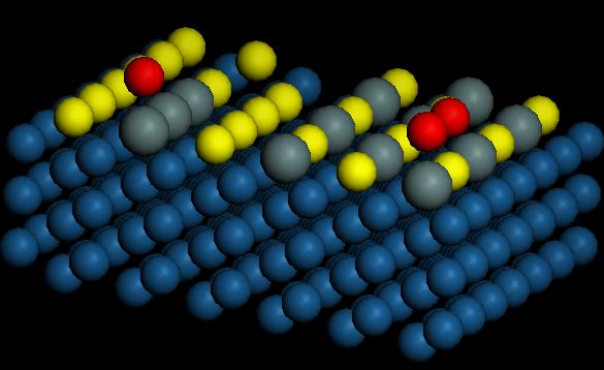


Figure 5.13 STM image of Pt₃Sn(110) single crystal after annealing to 1000 K. 120 Å, 0.5 V, 0.8 nA. Adopted from reference⁴⁰.

According our atomic assignment, the structure models of the 2.7-ML Sn/Pt(110) corresponding the LEED pattern were proposed and showed in Table 5.1. The accuracy of those models has not been verified and should be done by further theoretical calculation.

Table 5.1 Proposed models for each alloy surfaces

<p>Pt(110) :</p> <p>(1×2) LEED</p>		<p>Red: top Pt</p> <p>Yellow: second layer Pt</p>
<p>Sn/Pt(110) :</p> <p>(4×1) LEED</p>		<p>Gray: Sn</p>
<p>Sn/Pt(110) :</p> <p>(6×1) LEED</p> <p>Bi-atomic row</p>		<p>Gray: Sn</p> <p>Red, yellow, orange: Pt</p>
<p>Sn/Pt(110) :</p> <p>(6×1) LEED</p> <p>prism-like</p>		<p>Gray is Sn</p> <p>Red, Yellow: Pt</p>
<p>Sn/Pt(110):</p> <p>(1×1) LEED</p> <p>Anneal to 1050 K</p>		<p>Gray is Sn</p> <p>Red, Yellow: Pt</p>

5.4 Conclusions

This is the first time that the Sn-Pt(110) surface alloy formation process was observed and revealed in detail. When a high coverage of Sn was deposited to a clean Pt(110) single crystal surface, the Sn atoms would alloy with Pt rapidly leaving a rough surface. As the surface being annealed to higher temperature, Sn dissolved into the crystal bulk and several distinguished surface structures matching with their LEED pattern evolution path were observed. The final stage of annealing to 1050 K showed a surface morphology analogue to the Pt₃Sn(110) bulk alloy crystal, which confirms the validity of our research.

Chapter 6 Conclusions

In conclusion, the structures and alloying pathway of Sn/Pt(110) system were examined using surface science techniques such as LEED, XPS, AES, LEIS and STM. It is found that, unlike the stable Pt(111) surface, Pt(110)-(1×2) surface reacts with deposited Sn rapidly to form the room temperature alloy. This will happen on all circumstances, from low coverage to high coverage. Differ from what was found on the low Sn coverage system, the Sn-Pt(110) surface alloy obtained by exposure to more than 2 ML of Sn has distinct structures that corresponding to (4×1) and (6×1) LEED patterns. (2×2) surface alloy consistence with that found on Pt₃Sn(110) bulk single crystals will be formed ultimately when the annealing temperature is high enough. Annealing the alloy samples causes the surface Sn signal decrease for both medium and high coverage systems.

Those temperature- and coverage-dependent surface alloys may have potential application for chemical reactions. Further investigation of their chemistry properties, such as reactivity, selectivity, stability, *etc.* should be implemented and is our next goal. A theoretical calculation should also be accomplished in order to validate our proposed modes and the atomic assignments.

References

1. Paffett, M. T.; Windham, R. G., Surface modification of Pt(111) by Sn adatoms: Evidence for the formation of ordered overlayers and surface alloys. *Surf. Sci.* **1989**, 208, (1-2), 34-54.
2. Overbury, S. H.; Mullins, D. R.; Paffett, M. T.; Koel, B. E., Surface structure determination of Sn deposited on Pt(111) by low energy alkali ion scattering. *Surf. Sci.* **1991**, 254, (1-3), 45-57.
3. Paffett, M. T.; Logan, A. D.; Simonson, R. J.; Koel, B. E., A multitechnique surface science examination of Sn deposition on Pt(100). *Surf. Sci.* **1991**, 250, (1-3), 123-138.
4. Li, Y.; Koel, B. E., Structural studies of Sn/Pt(100) surfaces: conditions for alloy formation. *Surf. Sci.* **1995**, 330, (2), 193-206.
5. Zhao, H.; Koel, B. E., Hydrogenation of 1,3-butadiene on two ordered Sn/Pt(111) surface alloys. *J. Catal.* **2005**, 234, (1), 24-32.
6. Olivas, A.; Jerdev, D. I.; Koel, B. E., Hydrogenation of cyclohexanone on Pt-Sn surface alloys. *J. Catal.* **2004**, 222, (2), 285-292.
7. Panja, C.; Saliba, N.; Koel, B. E., Adsorption of methanol, ethanol and water on well-characterized Pt--Sn surface alloys. *Surf. Sci.* **1998**, 395, (2-3), 248-259.
8. Zhao, H.; Koel, B. E., Adsorption and reaction of bicyclic hydrocarbons at Pt(111) and Sn/Pt(111) surface alloys: trans-decahydronaphthalene (C₁₀H₁₈) and bicyclohexane (C₁₂H₂₂). *Surf. Sci.* **2004**, 573, (3), 413-425.
9. Xu, C.; Koel, B. E., Dehydrogenation of cyclohexene on ordered Sn/Pt(111) surface alloys. *Surf. Sci.* **1994**, 304, (3), 249-266.
10. Peck, J. W.; Mahon, D. I.; Koel, B. E., A temperature programmed desorption study of the reaction of methylacetylene on Pt(111) and Sn/Pt(111) surface alloys. *Surf. Sci.* **1998**, 410, (2-3), 200-213.
11. Tsai, Y.-L.; Xu, C.; Koel, B. E., Chemisorption of ethylene, propylene and isobutylene on ordered Sn/Pt(111) surface alloys. *Surf. Sci.* **1997**, 385, (1), 37-59.
12. Paffett, M. T.; Gebhard, S. C.; Windham, R. G.; Koel, B. E., Chemisorption of ethylene on ordered Sn/Pt(111) surface alloys. *Surf. Sci.* **1989**, 223, (3), 449-464.

13. Breitbach, J.; Franke, D.; Hamm, G.; Becker, C.; Wandelt, K., Adsorption of benzene on ordered Sn/Pt(111) surface alloys. *Surf. Sci.* **2002**, 507-510, 18-22.
14. Bodke, A. S.; Olschki, D. A.; Schmidt, L. D.; Ranzi, E., High Selectivities to Ethylene by Partial Oxidation of Ethane. *Science* **1999**, 285, (5428), 712-715.
15. De Santis, M.; Gauthier, Y.; Tolentino, H. C. N.; Bihlmayer, G.; Blugel, S.; Langlais, V., Structure and magnetic properties of Mn/Pt (110) - (1X2) : A joint x-ray diffraction and theoretical study. *Phys. Rev. B* **2007**, 75, (20), 205432.
16. Lundgren, E.; Alvarez, J.; Torrelles, X.; Peters, K. F.; Isern, H.; Ferrer, S., Co/Pt(110) interface: An x-ray-diffraction study. *Phys. Rev. B* **1999**, 59, (3), 2431.
17. Giordano, H.; Galeotti, M.; Cortigiani, B.; Torrini, M.; Bardi, U., Growth mechanism and epitaxy of cobalt on the Pt(110) surface. *Surf. Sci.* **1996**, 352-354, 870-874.
18. Alnot, M.; Fusy, J., Study of cobalt films deposited on Pt(110)(1X2). *Appl. Surf. Sci.* **1992**, 55, (2-3), 209-219.
19. Shern, C. S.; Tsay, J. S.; Fu, T.-y., Growth mechanism of Ni on Pt(110) at low temperature. *Appl. Surf. Sci.* **1996**, 92, 74-78.
20. Fu, T. I.; Liao, P. C.; Shern, C. S., Growth mechanism and surface alloy formation of Ni on Pt(110) surface. *J. Vac. Sci. Technol., A* **1993**, 11, (5), 2407-2410.
21. He, Y. L.; Zuo, J. K.; Wang, G. C.; Low, J. J., Diffusion of Rh overlayers grown on a Pt(110) surface. *Surf. Sci.* **1991**, 255, (3), 269-279.
22. Shern, C. S.; Chang, D. U.; Shyu, K. D.; Tsay, J. S.; Fu, T.-y., Initial growth of a silver thin film on a Pt(110)-(1X2) surface. *Surf. Sci.* **1994**, 318, (3), 262-266.
23. Janin, E.; von Schenck, H.; Hellden, S.; Tjernberg, O.; Karlsson, U. O.; Gothelid, M., Corrosive adsorption of Sn on the Pt(110)(1X2) surface. *Surf. Sci.* **2002**, 515, (2-3), 462-470.
24. UHV SPM, RHK brochure. http://www.scientek.com.tw/upload/rhk_uhv-subsystems.brochure.linear.pdf
25. Adams, D. L.; Nielsen, H. B.; Van Hove, M. A.; Ignatiev, A., LEED study of the Pt(110)-(1X2) surface. *Surf. Sci.* **1981**, 104, (1), 47-62.
26. Heinz, K.; Barthel, A.; Hammer, L.; Muller, K., Kinetics of the irreversible transition Pt(110)1X1-->1X2 as observed by LEED. *Surf. Sci.* **1987**, 191, (1-2), 174-184.

27. Wang, Z. RHK Variable Temperature Sample Holder With Built-in Quartz Lamp Heater. http://www.rhk-tech.com/media/tech_briefs/SampleHolder_QuartzHeater.pdf
28. Ertl, G.; Kuppers, J., *Low energy electrons and surface chemistry*. VCH: 1985.
29. Watts, J. F.; Wolstenholme, J., *An introduction to surface analysis by XPS and AES*. J. Wiley: 2003.
30. Woodruff, D. P.; Delchar, T. A., *Modern Techniques of Surface Science*. Cambridge University Press: 1994.
31. Cumpson, P. J.; Seah, M. P., Elastic Scattering Corrections in AES and XPS. II. Estimating Attenuation Lengths and Conditions Required for their Valid Use in Overlayer/Substrate Experiments. *Surf. Interface Anal.* **1997**, 25, (6), 430-446.
32. Brongersma, H. H.; Draxler, M.; de Ridder, M.; Bauer, P., Surface composition analysis by low-energy ion scattering. *Surf. Sci. Rep.* **2007**, 62, (3), 63-109.
33. Salmeron, M.; somorjai, G. A., A LEED-AES study of the reconstructed Pt(110) surface and the effect of oxygen treatment. *Surf. Sci.* **1980**, 91, (2-3), 373-384.
34. Bauer, E., Epitaxy of metals on metals. *Applications of Surface Science* **1982**, 11-12, 479-494.
35. Jackman, T. E.; Davies, J. A.; Jackson, O. P.; Unertl, W. N.; Norton, P. R., The Pt(110) phase transitions: A study by rutherford backscattering, nuclear microanalysis, LEED and thermal desorption spectroscopy. *Surf. Sci.* **1982**, 120, (2), 389-412.
36. Niehus, H., Analysis of the Pt(110)-(1X2) surface reconstruction. *Surf. Sci.* **1984**, 145, (2-3), 407-418.
37. Tomanek, D.; Brocksch, H. J.; Bennemann, K. H., Calculation of the structural energy of the unreconstructed and (1X2) reconstructed Pt(110) surface. *Surf. Sci. Lett.* **1984**, 138, (1), L129-L136.
38. Gritsch, T.; Coulman, D.; Behm, R. J.; Ertl, G., A scanning tunneling microscopy investigation of the structure of the Pt(110) and Au(110) surfaces. *Surf. Sci.* **1991**, 257, (1-3), 297-306.
39. Agnoli, S.; Orzali, T.; Sambì, M.; Vittadini, A.; Casarin, M.; Granozzi, G., Ultrathin TiO₂ Films on (1X2)-Pt(110): a LEED, Photoemission, STM, and Theoretical Investigation. *J. Phys. Chem. C* **2008**, 112, (50), 20038-20049.

40. Hoheisel, M.; Speller, S.; Kuntze, J.; Atrei, A.; Bardi, U.; Heiland, W., Structure of Pt₃Sn(110) studied by scanning tunneling microscopy. *Phys. Rev. B* **2001**, 63, (24), 245403.

Vita

Jie Fu was born Jan 1985 in Shanxi, China. She graduated from Shandong University in Jinan, Shandong in July 2006 with a Bachelor's degree of Science in Chemistry. She then went to Department of Chemical Engineering of Sungkyunkwan University in Suwon, South Korea. She obtained her Master's degree of Chemical Engineering in August 2008. Jie was then admitted by Lehigh University, PA and joined back to the Chemistry Department. During the study at Lehigh, she was a teaching assistant for several labs and a research assistant in Prof. Bruce Koel's surface science group. Her research interests include the surface structure of Pt-Sn system and transition metal oxides as potential photocatalysts.